
Study of Magnetic Core Losses in Soft Magnetic Materials for AC Applications

*Thesis Submitted to Midnapore City College
for the Partial Fulfillment of the Degree of
Master of Science (physics)*

Submitted by

**Avinash Bera, Suravi Nayek
and Souvik Barman**

Guided by

Dr. Subhendu Kumar Manna
(Assistant Professor in Physics)



Department of pure and applied sciences
MIDNAPORE CITY COLLEGE
Kuturiya, P.O. Bhadutala,
Paschim Medinipur, Pin-721129
West Bengal, India
2023

Declaration

I do hereby declare that the present Master thesis entitled '*Study of Magnetic Core Losses in Soft Magnetic Materials for AC Applications*' embodies the original research work carried out by me in the Department of pure and applied sciences, Midnapore City College, Paschim Medinipur, West Bengal, India under the supervision of Dr. Subhendu Kumar Manna, Assistant Professor in Physics, Midnapore City College, Kuturiya, P.O. Bhadutala, Paschim Medinipur, Pin-721129, West Bengal. No part thereof has been submitted for any degree or diploma in any University.

Date:

Place: Midnapore City College, Paschim Medinipur

Suravi Nayek

Avinash Bera

Souvik Barman

Approval Sheet

This project report entitled by “*Study of Magnetic Core Losses in Soft Magnetic Materials for AC Applications*” Suravi Nayek is approved for the degree of *Master of Science (physics)*

(Signature of Examiners)

(Name:)

(Signature of Guide)


(Name: Dr. Subhendu Kumar Manna)

(Signature of Principal/Teacher-In-charge)

(Name: Dr. Kuntal Ghosh)

(Signature of Director)

(Name: Dr. Pradip Ghosh)



Dedicated to my Parents

Acknowledgement

I would first like to acknowledge Dr. Pradip Ghosh, Hon'ble Founder Director, Midnapore City College, Paschim Medinipur for providing me the opportunity to study and complete my thesis work in this college. I am gratefully indebted to him for his very valuable comments on this thesis.

I would like to thank my thesis advisor Dr. Subhendu Kumar Manna of the Physics Department at Midnapore City College. The door to Prof. Manna office was always open whenever I ran into a trouble spot or had a question about my research or writing. He consistently allowed this paper to be my own work, but steered me in the right the direction whenever he thought I needed it.

I would also like to thank the other Faculties Dr. Atanu Das, Dr. Saptarshi De, Dr. Subhendu Kumar Manna and other non-teaching staffs for their support to carry out this research project. Without their passionate participation and input, the validation survey could not have been successfully conducted.

Finally, I must express my very profound gratitude to my parents for providing me with unfailing support and continuous encouragement throughout my years of study and through the process of researching and writing this thesis. This accomplishment would not have been possible without them. Thank you.

Suravi Nayek

Avinash bera

Souvik Barman

Abstract

In modern day technology the magnetic components are fundamental element and represent one of the greatest challenges for designers because there are some components that lead the opposition due to losses (both electrical and thermal), which indeed hinders to achieve the desirable energy density. The use of soft ferromagnetic materials as substitutes for ferrite in the core of magnetic components has been proposed as a solution to this problem. With those, a new perspective and methodology in the calculation of power losses have been opened up to design advanced energy transfer devices and overcome the challenges in this field. The core materials used to build such energy devices, such as-power inductors and transformers, are soft magnetic materials. When there is an alternating external field, the magnetic moments rotate and consume energy, which is the core loss. The core loss depends on the AC flux frequency, amplitude, waveform, DC bias and temperature. These dependences are nonlinear and difficult to predict. Several research groups are giving huge efforts from last few decades to predict these losses and establish an unique model, which would be useful for all types of core materials. However, achieving a core losses model that combines all the parameters (electric, magnetic, thermal) needed in power electronic applications is a challenge. Therefore, the main objective of this project is to critical scrutiny the existing core loss models with the help of experimental results obtained in this work. Also, effort has been given to find the reason behind the excess loss in the studied sample and try to minimize the losses in the ferromagnetic material. The coercivity (H_C), permeability (μ_r), magnetic core losses and other soft magnetic parameters of an industrially available ferromagnetic alloy (Fe-P-Si) have been studied with the help of B-H loop tracer. Result of this project work provides, in one source, tools and techniques to develop more efficient soft magnetic materials and way to reduce the core losses due to altering in the magnetization.

List of Tables

TABLE NAME	PAGE NO.
Table 1.1: Curie Temperatures for Some Ferromagnetic and Ferrimagnetic Materials	3
Table 1.2. Some Famous Industrial Materials and Their Parameters	15
Table 1.3: Some Famous Industrial Material Core Loss	24
Table 5.1(a): Data chart for Frequency dependent coercivity in Fe-P-Si	46
Table 5.1(b): fitting parameters for equation (25)	49
Table 5.1(C): data for fitting parameter in H_c vs frequency curve for eq (26)	50
Table: 5.2:data table for relative permeability	69
Table:5.3: Data frequency and total core	61

List of Figures

PICTURE NAME	PAGE NO.
<i>Figure 1.1: Classification of magnetism</i>	2
<i>Figure 1.2 (i): Diagram of magnetic domains with minimization of magnetostatic energy. H_s</i>	4
<i>Figure 1.2(ii): Domain arrangements for various status of magnetization</i>	6
<i>Figure 1.3(i) A typical major hysteresis loop. From demagnetized state at 0 to the saturation state</i>	9
<i>Figure 1.3.2(ii): Minor loops (a) and first order reversal curves (FORCs) (b) in major loops</i>	10
<i>Figure 1.4: A magnetic hysteresis loop for soft and hard ferromagnetic material</i>	11
<i>Figure 1.5. A typical picture of magnetic core</i>	16
<i>Figure 1.6: Types and classification of losses presented on magnetic components</i>	17
<i>Figure 1.6.2(i): Eddy currents inside a metal block. Flux view of the partial core</i>	20

<i>Figure 1.6.2(ii): Two rectangular billets with different lamination orientations</i>	22
<i>Fig. 1.6.3: Division of total No- Load loss into Its Component</i>	24
<i>Figure 4: Different core loss model for calculate loss separation in magnetic core</i>	36
<i>Figure 4.4(i). Ac hysteresis loop</i>	40
<i>Figure 4.4(ii). Core loss measurement electromagnetic circuit</i>	40
<i>Figure 4.4 (iii) Donart testing equipment</i>	41
<i>Figure 4. (iv) Test bench testing equipment</i>	42
<i>Figure 4.4 (v) Test bench schematic</i>	43
<i>Figure 5.1(i): Fitting on the frequency dependent coercivity on different magnetic field on Fe-P-Si according eq (254) (a)$B=0.65$, (b)$B= 0.45T$, (c)$B=1T$, (d)$B=1.25T$</i>	48
<i>Figure 5.1(ii): Fitting on the frequency dependent coercivity on different magnetic field on Fe-P-Si according eq (26)</i>	49
<i>Figure 5.2: Magnetic hysteresis measurements at DC</i>	51

<i>Figure 5.3 (a): Magnetic hysteresis measurements at 0.45T, Swelling-up of hysteresis with frequency</i>	52-53
<i>Figure 5.3 (b): Magnetic hysteresis measurements at 0.65T, Swelling-up of hysteresis with frequency</i>	54-55
<i>Figure 5.3 (c): Magnetic hysteresis measurements at 1T, Swelling-up of hysteresis with frequency</i>	55-56
<i>Figure 5.3 (d): Magnetic hysteresis measurements at 1.25T, Swelling-up of hysteresis with frequency</i>	56-57
<i>Figure.5.4 frequency vs relative permeability curve fitting</i>	60
<i>Figure 5.5(a): Fitting data on basis of equation (31), frequency vs core loss</i>	62
<i>Figure 5.5(b): Fitting data on basis of equation (31), frequency vs core loss</i>	63
<i>Figure 5.5(c): Steinmetz and Classical Model Comparison</i>	64
<i>Figure 5.5(d): Fitting data on basis of equation (32), Improve core loss models</i>	65
<i>Figure 5.5(d): Steinmetz, Classical Model and improve core loss model Comparison</i>	66

Table of Contents

CONTENTS	PAGE No.
1. Introduction	1-25
<i>1.1. Theoretical Background</i>	4
<i>1.2. Magnetization and Domain Distribution</i>	7 10
<i>1.3. Hysteresis Loops</i>	
<i>1.4. Types of Magnetic Materials Based on Hysteresis Loops</i>	15
<i>1.5. Soft Magnetic Core</i>	17
<i>1.6 Core Losses</i>	25
2. Literature review	26-31
3. Aims and Objective	32-33
4. Material and Methods	34-43
<i>4.1 Mathematical Models</i>	37
<i>4.2 Loss Separation Models</i>	37
<i>4.3. Empirical Models</i>	38
<i>4.4 Core Loss Modeling</i>	43

5. Results	44-66
5.1 <i>Study on Frequency dependent coercivity</i>	45
5.2 <i>DC Hysteresis</i>	50
5.3. <i>Frequency Depended Hysteresis</i>	58
5.4. <i>Frequency Dependance Relative Permittivity</i>	60
5.5. <i>Frequency dependent Total losses:</i>	61
6. Discussion	67-73
6.1. <i>Discussion Frequency dependent coercivity:</i>	68
6.2. <i>Discussion DC hysteretic behavior</i>	68
6.3 <i>Discussion on ac Hysteretic Behavior</i>	69
6.4 <i>Discussion on relative permeability</i>	70
6.5 <i>Discussions Frequency dependent Total losses</i>	71
7. Conclusion	74-75
8. Future outcome	76-77
8. References	78-84

CHAPTER 1: INTRODUCTION

1. Introduction

It is a fact that magnetic components are an essential part of our lives. We can find them in almost anything of our daily use from simple things such as cell phone charges to TVs and home appliances. However, they have become more relevant in the development of electric and hybrid vehicles, electric machines, renewable energy systems. Inside these devices and systems, a power stage is confirmed by magnetic and electronic components. A few years ago, these power stages used to be bigger and heavier, and they had considerable energy losses making them less efficient. Nowadays, silicon carbide (SiC) and gallium nitride (GaN) switching devices have improved power electronics, making them smaller and faster. In a modern power converter, magnetics are approximately half of the volume and weight, and they are the main source of power losses

1.1 Theoretical Background:

Ferromagnetism and Ferromagnetic materials are widely applied attributing to their strong magnetism. To characterize and simulate the magnetic behavior of ferromagnetic materials, it is necessary to understand the physical background of ferromagnetism.

Classification of Magnetism:

In physics, according to different magnetic behavior, substances are classified as diamagnetic, paramagnetic, or ferromagnetic, etc. [Cullity and Graham, 2011]. As shown in [Figure.1.1], magnetic orders and temperature dependency vary in different types of substances. In comparison with strong ferromagnetism and ferrimagnetism, Paramagnetism and diamagnetism exhibit a weak response to an external magnetic field, which can only be detected by sensitive instruments.

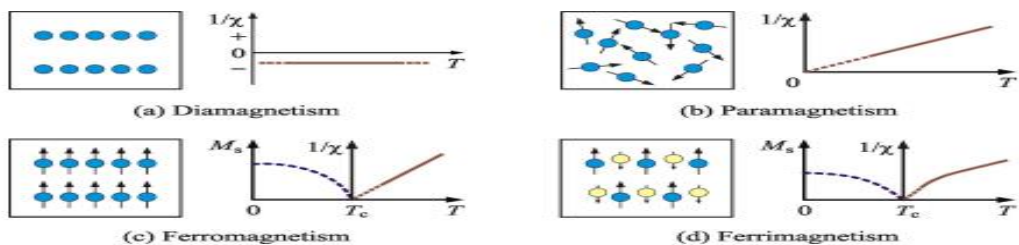


Figure1.1: Classification of magnetism. T is temperature, χ is the magnetic susceptibility, M_s is the spontaneous magnetization. In (c) and (d) substances are in zero applied field within a single domain (below T_c), and in a group of atoms (above T_c) source: [Cullity and Graham, 2011].

Table 1.1: Curie Temperatures for Some Ferromagnetic and Ferrimagnetic Materials

Ferromagnetic		Ferrimagnetic	
Substance	T _c (K)	Substance	T _c (K)
Ni	627	MnFe ₂ O ₄	573
Fe	1043	NiFe ₂ O ₄	858
Co	1388	BaOFe ₂ O ₃	723
Gd	292	Y ₃ Fe ₅ O ₁₂	523

Diamagnetic materials exhibit negative magnetism, which is independent of temperature [see **Figure.1.1(a)**]. As another weak magnetism, Para magnetism exhibits relatively strong temperature dependency [see **Figure. 1.1(b)**]. According to the Curie law,

$$\chi = \frac{M}{H} = \frac{C}{T} \quad (1)$$

where C is the Curie constant per gram [Cullity and Graham, 2011]. The distribution of magnetic moments is disordered, which is due to the disturbance of thermal energy [Tumanski, 2011]. When temperature increases, the susceptibility decreases linearly. Compared with paramagnetic material, ferromagnetic material exhibits strong magnetism even in the absence of an external magnetic field. It is due to spontaneous magnetization resulting from interatomic exchange interaction [Tumanski, Chikazumi and Graham, 2009]. As is shown in [Figure **1.2(i), (c)**] spontaneous magnetization (M_s) decreases with the increase of temperature. Above a certain temperature (T_c), ferromagnetic materials begin to exhibit paramagnetic behavior, where the susceptibility χ of ferromagnetic material is described in Curie-Weiss law,

$$\chi = \frac{C}{T-T_c} \quad (2)$$

where T_c is the boundary temperature and called Curie temperature. In **Table.1.1** the Curie temperature of some ferro- and ferrimagnetic materials are listed. It is an important parameter in design of equipment and metal processing.

In [Figure. 1.1(d)], it can be seen that like ferromagnets, ferrimagnetic materials exhibit spontaneous magnetization below the Curie temperature, but become paramagnetic above it. However, there are two different sublattices in ferrimagnetic materials shown in magnetic orders of [Figure. 1.1(d)]. On different sublattices the magnetic moments are opposed but not equal, which leads to a spontaneous magnetization in ferrimagnetic materials. In industry, ferrites are important materials alongside ferromagnets. In addition to their economic advantage, they are mostly applied in high-frequency conditions due to their high resistivity. Where T_c is the boundary temperature and called Curie temperature. In Table.1.1 the Curie temperature of some ferro- and ferrimagnetic materials are listed. It is an important parameter in design of equipment and metal processing. In [Figure. 1.1(d)], it can be seen that like ferromagnets, ferrimagnetic materials exhibit spontaneous magnetization below the Curie temperature, but become paramagnetic above it. However, there are two different sublattices in ferrimagnetic materials shown in magnetic orders of [Figure. 1.1(d)]. On different sublattices the magnetic moments are opposed but not equal, which leads to a spontaneous magnetization in ferrimagnetic materials. In industry, ferrites are important materials alongside ferromagnets. In addition to their economic advantage, they are mostly applied in high-frequency conditions due to their high resistivity.

1.2. Magnetization and Domain Distribution:

Magnetic Domains:

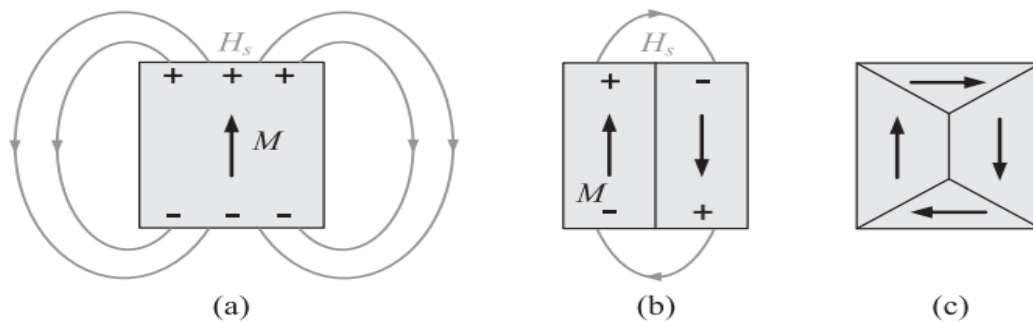


Figure 1.2 (i): Diagram of magnetic domains with minimization of magnetostatic energy. H_s in (a) is the stray field caused by spontaneous magnetization in magnet, (b) the formation of domain structure reduces the magnetic energy, (c) with multiple domains the whole magnetization is zero, the magnet is in minimum energy state [Hamann, 2010].

As mentioned in the previous ferromagnetic materials still exhibit magnetization even in the absence of an external magnetic field. However, ferromagnetic materials can be

demagnetized despite the internal “molecular field” [Weiss, 1907]. To explain this phenomenon, Pierre Weiss assumed that material is divided into many small regions (about 1-100 μm), which exhibits spontaneous magnetization in different directions. The small regions are known as domains, and the boundaries between different domains are called domain walls. When material is demagnetized, multiple domains are formed, which results in zero net magnetization see [Figure. 1.2(i), (c)]. In saturation state, most of the domains are oriented along the external field direction.

When a ferromagnet or a ferrimagnetic material is heated above its Curie temperature, the uniform magnetization within a domain spontaneously disappears. Each atom has its own direction of magnetic moment, which leads to paramagnetic behavior. In 1935, it was mathematically proved that domains form to ensure the lowest magnetostatic energy [Landau and Lifshitz, 1935]. In 1949 the domain structure in silicon-iron single crystals was published by H. J. Williams, R. M. Bozorth, and W. Shockley [Williams, Bozorth, and Shockley, 1949]. This was considered as direct experimental evidence of the domain theory. Since that time, domain theory has been essential in explaining the shape of a magnetization curve or the mechanism of magnetic hysteresis [Cullity and Graham, 2011; Tumanski, 2011]

When a ferro- or ferrimagnetic material is placed in an increasing magnetic field, its net magnetization is increased up to a limited value called the saturation magnetization. This process is called technical magnetization as the increase in net magnetization is not the same as a change in intensity of the spontaneous magnetization in [Figure. 1.1(c) and (d)]. During the technical magnetization the net magnetization is changed by domain wall displacement and by rotation of domain magnetization [Chikazumi and Graham, 2009]

[Figure. 1.2(ii)] presents domain arrangements in different states of magnetization. Suppose the magnetization starts from a fully demagnetized state, then it is at the origin 0 in [Figure. 1.3]. When a small positive magnetic field is applied, as shown at points 1 and 2, the domains whose direction of spontaneous magnetization is close to the direction of the applied field start to grow. At the same time, the other domains are gradually eliminated. When the applied magnetic field is further increased, most of magnetizations are lined up almost in parallel as shown at point 3. Finally, the net magnetization changes to a lesser degree with the increase of an applied field. The magnetization is realized by rotation of

the direction of magnetization. As shown at point 4, it is at saturation state. The curve from the demagnetized state to saturation (path 0 – 4) is called the primary magnetization curve [Tumanski, 2011] or normal induction curve [Cullity and Graham, 2011]

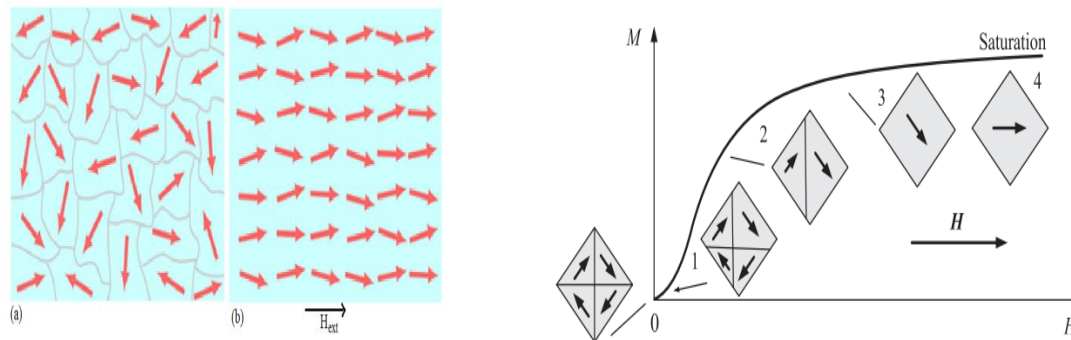


Figure 1.2(ii): Domain arrangements for various status of magnetization [Tumanski, 2011]. The material is in demagnetized state at 0. When the applied magnetic field increases, the magnetization increases along the path 0-1-2-3-4 until saturation state

Ferromagnetic materials such as the transition elements Iron (Fe), Nickel (Ni), Cobalt (Co), and rare earth metals like Gadolinium (Gd), Terbium (Tb), Dysprosium (Dy), Holmium (Ho), and Erbium (Er), are “spontaneous magnetized” by a parallel alignment of magnetic moments even in absence of external magnetic field. This magnetic ordering occurs due to exchange which can be only explained by quantum mechanics. From “outside” this magnetic behavior cause a magnetic Hysteresis measuring the magnetization as function of the magnetic field. Such a hysteresis is caused by the movement and alignment of magnetic domains. The parallel alignment of magnetic moments in one direction is subdivided into small regions (microscopic) within a material, known as domains in order to minimize the magnetostatic stray field energy of the system. Adjacent domains are separated by domain boundaries or walls called Bloch walls (180° walls) or Neel walls (90° walls) in which the direction of the magnetic moment gradually and continuously changes from that of one domain to adjacent domains. The thickness of the domain wall is much smaller than the domains itself and roughly proportional to the $p A/K$ (A -exchange stiffness constant, K -anisotropy energy). Different energy contributes to the formation of domains and determine its size i.e., magnetostatic (stray field) energy, crystal anisotropy, magnetoelastic energy etc. Normally the domain size can range from a few micrometers to 1 mm in a demagnetized material as whole. Nevertheless, the parallel arrangements of magnetic moments within domains depend on the ambient temperature. At the Curie temperature (depends on

the type of ferromagnetic materials), the parallel alignment of moments breaks down because of thermal agitation and the material is no more ferromagnetic. In the absence of external field $H_{\text{ext}}=0$, the domains are oriented in random directions such that the net magnetization of material as a whole become zero as shown in [Figure 1.2(ii)]. When a demagnetized ferromagnetic material well below the Curie temperature (having a net magnetization zero) is brought into an external magnetic field, the domains lying more or less in the direction of the applied field start to grow at the expense of other domains until most favorably oriented domains remains when the external field is high enough. Further increase in the magnetic field causes the domains to rotate and align parallel to the applied field. At this stage the material is saturated as shown in [Figure 1.2(ii)] During the growth of magnetic domains there has been no change in the magnitude of the local magnetization only the domain walls move and the external field provides the force required for this movement.

1.3 Hysteresis Curves and Magnetic Properties:

The hysteresis loop expresses a nonlinear, irreversible relationship between the magnetic flux density B and the applied magnetic field H_{ext} . Generally, the external field has to be corrected for demagnetizing field effects. Only in the case of a magnetically closed circuit the external field is equal to the internal field. A typical hysteresis loop for a ferromagnetic material as shown in [Figure. 1.3(i)] Hysteresis refers to the lagging of the magnetization of ferromagnetic material. Not all the energy of the magnetic field is returned to the circuit when magnetic field is removed. It is known as hysteresis loss. The core of a transformer is subjected to an AC force and for each cycle of e.m.f, a hysteresis loop is traced out. A great deal of information can be learned about the magnetic properties of a material by studying its hysteresis loop [Parthasaradhy and Kulu, 2014]. There are two kinds of Hysteresis loop possible in a ferromagnetic material.

1.3.1 Major Hysteresis Loops:

After saturation has been reached in Fig.1.2(ii), if the applied magnetic field is removed, the magnetization will not return back to zero. Instead, there is still some magnetization left in the material. To drive the magnetization back to zero, a field in the opposite direction should be applied to the material. This behavior is called magnetic hysteresis. It is

considered as typical symbol of magnetism and an important character of magnetic properties [Bertotti, 1998].

A hysteresis loop is a plot showing the variation of magnetization with magnetic field. In material catalogues it is normally in terms of the flux density B (or the polarization J) and the magnetic field strength H . According to (1.2(ii)), H forms part of B , after saturation, a constant M_s is reached, but B continues to increase with magnetic field H [Cullity and Graham, 2011].

$$B = \mu_0(H + M) \quad (3)$$

$$B = \mu_0(H) + J \quad (4)$$

where μ_0 is the permeability of free space. As shown in [Figure.1.3(i)], the magnetic flux density increases from the demagnetized state to saturation along the path 0-1. It is similar to the magnetization curve shown in [Figure.1.2(ii)], By measuring the primary magnetization curve the permeability of material μ can be obtained by

$$\mu(H) = \mu_0\mu_r(H) = \frac{B}{H} \quad (5)$$

where μ_r is known as relative permeability. If we start decreasing the magnetic field strength, due to an irreversible change of domain walls' locations, the return path is along the path 1-2 but not along the path 1-0. At zero magnetic field (point 2), there is a retentivity or residual induction B_r in the magnetic material. To decrease the flux density back to zero (point 3), a magnetic field is applied in the opposite direction. This field is called coercivity H_c . If we continue increasing the magnetic field in a negative direction, the negative saturation $-B_s$ will be reached (point 4). If the magnetic field returns back to zero then increases to reach the positive saturation state (point 1), the path 1-2-3-4-5-6 forms a closed loop known as the major hysteresis loop.

Parts of major loops:

- 1) Point O (origin) presents the demagnetized, initial state of the material, with increasing applied field (H_{ext}) in positive direction, the favorable domains of the material start to increase in the direction of H_{ext} as shown in Figure from O to a
- 2) When the external field H_{ext} is sufficiently high, the induction $B(H)$ in the material becomes saturated ($+B_s$) by aligning all domains in the direction of H_{ext} and a further

increase in the external field produce no significant change in the magnetic induction B . The first $B(H)$ curve from the demagnetized state “O” to the saturation point B_s is called “virgin curve” of the $B(H)$ hysteresis.

- 3) After saturation, when the external field (H_{ext}) is reduced to zero the magnetic induction B does not reduce to zero but it retains in a remanent state which is known as remanence ($+B_r$). This is valid in a magnetically closed system.

Now to demagnetized the material that means to reduce B_r to zero, the external field H_{ext} has to be applied in the negative direction. This negative value of H_{ext} where the induction B becomes zero is described by H_c and is called coercive force or coercivity. A further increase of H_{ext} in the negative direction can saturate the material but in the opposite direction ($-B_s$). If now the negative H_{ext} field reduces to zero the material achieves again a remanent magnetization ($-B_r$). The hysteresis loop traced out from $+B_s$

- 4) to $-B_s$ is called the major hysteresis loop. If the field H_{ext} is not sufficient to saturate the sample also a loop is formed which is called minor loop.

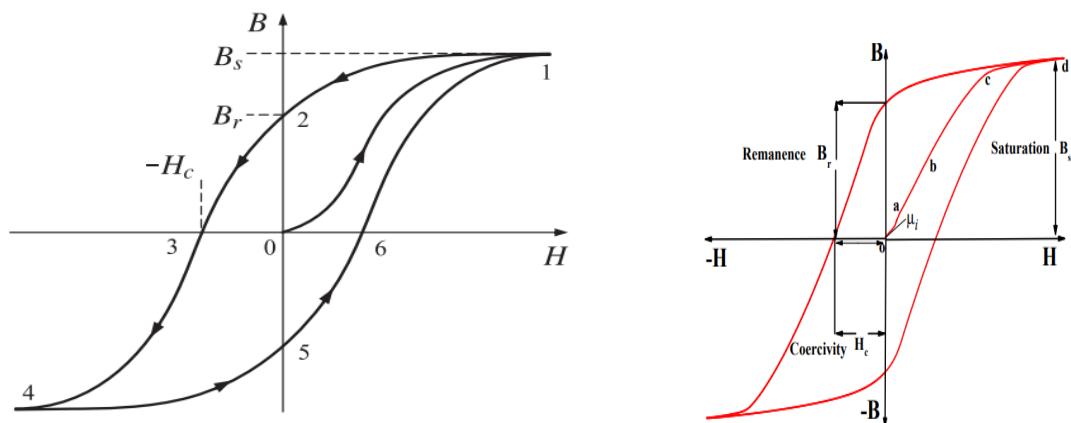


Figure.1.3(i): A typical major hysteresis loop. From demagnetized state at 0 to the saturation state B_s at 1, the 0–1 path form as a primary magnetization curve. When $H = 0$, the magnetic flux at 2 is the remanent flux density B_r . To decrease the magnetic flux back to zero, coercive field strength H_c in negative direction is applied. The path 1-2-3-4-5-6-1 forms a major hysteresis loop. [Cullity and Graham,

1.3.2 Minor Hysteresis Loops and FORCs:

In the primary magnetization process, if a reverse happens at some intermediate point before saturation, such as point a in [Figure 1.3.2(i)], a small closed loop can be obtained inside the major loop. This can be achieved by symmetrically reversing the corresponding

field. As shown in Figure 1.3.2(i), the small loop whose tip is at point a is called a minor hysteresis loop. On this minor loop, the rest induction at point b is called remanence. The magnetic field at point c is called coercive field. They are named differently to the retentivity and coercivity of major loops [Cullity and Graham, 2011]. Besides symmetrical (symmetrical to origin) minor hysteresis loops (loop abc), asymmetrical minor loops can also be formed at points d and e inside the major loop in **[Figure 1.3.2(i)]**. In identification of hysteresis models (e.g., Preisach hysteresis model), as shown in **[Figure 1.3.2(i)]** first-order reversal curves (FORCs) are usually measured by decreasing the field at some points on the ascending major loop (or increasing the field at some points on the descending major loop) [Torre, 1999]. In AC field measurements, primary magnetization curves are produced by joining tips of minor loops. To achieve the demagnetized state, material is firstly magnetized to saturation. By applying a series of alternating fields with slowly decreasing amplitude, the induction of the material becomes smaller and smaller. Another demagnetization method is called thermal demagnetization. As mentioned, previous, when ferro- or ferrimagnetic material is heated above its Curie point, it becomes paramagnetic. After cooling it in the absence of a magnetic field, the material can be demagnetized [Cullity and Graham, 2011]

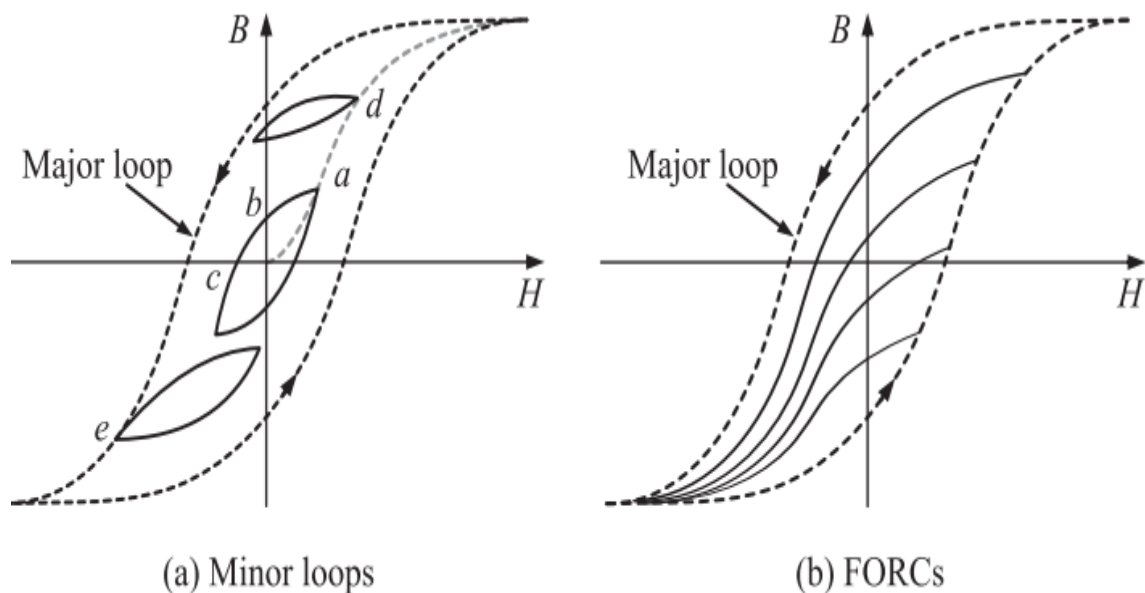


Figure 1.3.2(ii): Minor loops (a) and first order reversal curves (FORCs) (b) in major loops.

Source: [Cullity and Graham, 2011]

From application point of view magnetic materials can be classified as hard magnetic materials (Permanent Magnets) and Soft Magnetic Materials. This classification is made on the basis of coercive value. [Figure 1.4] illustrates the usual way to distinguish between two types of materials.

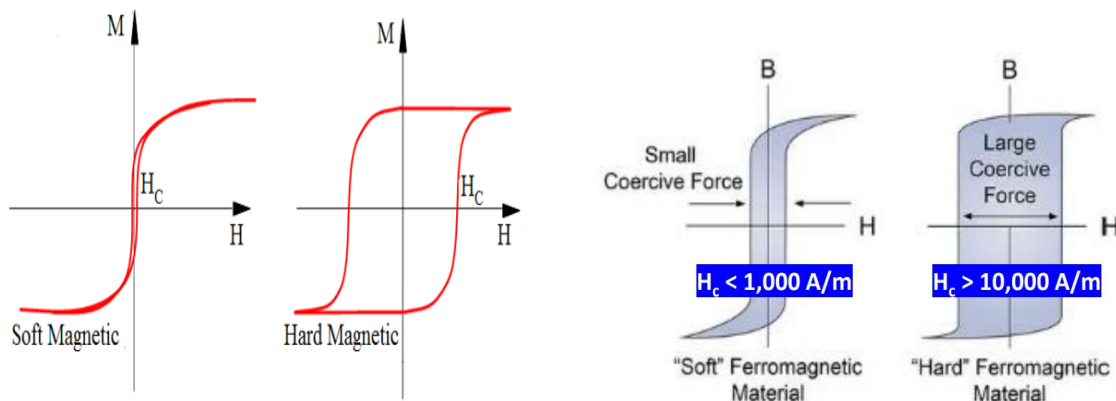


Figure1.4: A magnetic hysteresis loop for soft and hard ferromagnetic material,

source: (<https://www.electronics-tutorials.ws/electromagnetism/magnetic-hysteresis.html>)

1.4.1. Hard Magnetic Materials:

Materials with a high coercivity ($H_c > 10 \text{ kA/m}$) are considered as a hard magnetic material [Jiles, 1991]. Due to the high coercivity, a strong magnetic field is required to magnetize the material. Once such material being magnetized, they exhibit and retain a strong net magnetization without external field, that means that these materials not only have a high coercivity but also a high saturation (B_s) and remnant inductions (B_r) [McHenry & Laughlin, 2000]. These materials are used for permanent magnets in order to generate strong static fields (up to about 1T). Magnets used for different applications such as transforming energy from one form to another i.e., converting mechanical energy to electrical energy and vice versa for example generators, motors and microphones, loudspeakers etc. Engineers are more interested in a part of the hysteresis loop which lies in the second quadrant commonly called “Demagnetizing curve” in order to determine the suitability and performance of a permanent magnet for a particular device. Fe-carbon steel and special alloys such as Al- CO_{max} , Alnico, and Ticonal, which contain various amounts of aluminum, nickel, cobalt, and copper, are used to make low-cost permanent magnets. The strongest permanent magnets are nowadays rare earth intermetallic based on Sm-Co or Nd-Fe-B, produced by a sintering technology [Roderwald et al., 1989] [Taliyan, 2006]. Ceramics such as Ba- or Sr-ferrites are interesting for dynamic applications [Jancarik et al.,

2006]. They are produced using a wet chemical route (sol gel) and afterward sintered at high pressure and high temperatures from powders [Rodriguez and Fernandez et al., 2004] [Jafari et al., 2008]

1.4.2. Soft Magnetic Materials:

Properties desirable in a soft magnetic material: - large μ_i and μ_{max} - small H_s , small W_h , - large M_s (The magnetic materials having coercivity less than 1 kA/m are considered as magnetically soft. These materials are easy to magnetize and demagnetize. The main characteristics of soft magnetic materials are low core losses, high permeability and high induction. Depending on the application and its requirements, soft magnetic materials are selected on the basis of these characteristic. The most common application lies in transformers and generators which use soft magnetic Fe-3 wt%Si sheets [Gavrila et al., 2002]. High frequency applications of soft magnetic materials use soft magnetic ferrites: in all cases low core losses are required. Therefore, low coercivity combined with a high permeability and low magneto crystalline anisotropy are necessary for soft magnetic materials [Beatrice and fiorillo, 2006]. The most important conventional and new soft magnetic materials are given in the following list;

- a) Fe-Si alloys one of the most extensively used soft magnetic materials in electrical industry with typically operating frequency 50/60 Hz. The main applications for these soft magnetic materials are in generators, motors, transformers, electromagnets and relays. These applications need high-induction, low losses and high permeability magnetic materials. The most common material used for these applications is non oriented and oriented 3% silicon-iron but many smaller motors use silicon-free low carbon steel for economic reasons. Grain oriented iron-silicon alloys are mostly used for high energy transformers because of low core losses. High-frequency transformers use ferrites although this represents only a small volume of the total transformer market [Jiles, 1991]. The addition of nonmagnetic silicon in iron enhance its properties in many respects, most important is the increase of the electrical resistivity of the material due to the addition of Si into Fe for example, Fe-3 wt%Si has four-time higher resistivity than pure iron [Jiles, 1991]. Consequently, the dynamic losses due to eddy currents are reduced that's why it is suitable for transformers. Additionally, the magnetostriction decreases with increasing Si

content [Carr and Smoluchowski, 1951] [Tatsumoto and Okamoto, 1969] [Hall, 1959]. Also, this causes a reduction of the coercive field and the hysteresis losses. Consequently, the mechanical noise of operating transformers is reduced. From this magnetic point of view, the best composition is around 6-wt% Si which reduces the magneto crystalline anisotropy and the magnetostriction. This material has the highest permeability and the lowest coercivity, however it is too brittle for standard applications. Nevertheless, addition of silicon in iron also has two harmful effects: first it reduces the saturation magnetization, second it influences the mechanical workability. The reduction of the Curie temperature below 10-wt%Si is of no practical importance.

- b) Fe-Al alloys (“Sendust” FeSiAl) exhibit the lowest magneto crystalline anisotropy combined with a nearly zero magnetostriction. These alloys have a high resistivity, lower density and a higher hardness and a good resistance against corrosion which is better than those of nickel-iron and many other soft magnetic alloys as silicon-iron steel. That is why these alloys are more suitable for special environments such as nuclear radiation, shock, acceleration, etc. and also have significant industrial application in the fields of aviation, space flight, navigation, and other civilian and military industries. However due to higher costs than silicon-iron these alloys are unlikely to replace silicon-iron for general electrical applications. Additionally, this material is very brittle and needs special production methods which causes also additional costs.
- c) Soft magnet Iron-cobalt (Fe-Co) is the only alloy with increased saturation magnetization (up to 2.4 T) [Sourmail, 2004] as well as the highest Curie temperature of all other binary alloys with iron. The high saturation magnetization is about 2.45 T with 35-wt% Co. Therefore, this alloy is suitable for high induction application and elevated temperatures. The material is very corrosion stable. Drawback of these alloys is that they are mechanically very hard, furthermore cobalt is also expensive.
- d) Soft ferrites (Mn-Zn ferrites) are ceramic materials. Their chemical composition is (metal oxides) + (iron oxide)- MFe_2O_3 where M represents transition metal such as iron (Fe), manganese (Mn), magnesium (Mg), nickel (Ni), zinc (Zn).

Soft Magnetic Amorphous Materials:

Amorphous materials have no periodic arrangement of the atoms because they are produced by rapid cooling (quenching) of the molten alloys of usually Fe, Co, or Ni with a metalloid such as B, C, Si, P, or Al. Metalloid is added in order to stabilize the amorphous phase. An example of such an amorphous alloy is Fe₈₀B₂₀ (Met glass 2605). The amorphous alloys have usually excellent soft magnetic properties even in the as-cast state which exhibit a highly stressed state. Magnetic properties of amorphous materials are different from those found in their crystalline counterparts. The basic reason is that some magnetic properties are particularly structure sensitive that is why the properties of amorphous materials strongly depends on the fabrication process. In general, amorphous materials show excellent soft magnetic properties due to the averaging of magneto crystalline anisotropy and microstructural defects (grain boundaries, dislocations or precipitates) on which domain walls could be pinned even in the as-cast state.

The amount of work needed to be done to align the dipoles of the material parallel to the applied magnetic field is lost in the form of heat.

A good soft magnetic material exhibits minimal hysteresis with low magnetostriction, high polarization and the largest possible permeability. Permeability is usually referred to the internal field, because soft magnets tend to be used in a toroidal geometry.

For a ferromagnetic material, the magnetic induction B inside the sample is defined as:

$$B = \mu_0(H + M) \quad (6)$$

Where μ_0 is the permeability in free space and its value is $4\pi \times 10^{-7} \text{ Vs/Am}$ and M is the magnetization which is spontaneously induced in a ferromagnetic material by exchange and which becomes visible by applying field H_{ext} . In free space $M=0$ B and H are related as:

$$B = \mu_0\mu_r H_{ext} \quad (7)$$

Where μ_r is the relative permeability and in vacuum $\mu_r=1$.

In general, a material becomes magnetized as response to an external field H_{ext} and can be measured through its susceptibility and permeability. Hence, M can be expressed as,

$$M = \chi_m H_{ext} \quad (8)$$

Where χ_m is the magnetic susceptibility (unitless) “response function” of the magnetization of a material due to an applied magnetic field. Relative permeability and magnetic susceptibility are related as follows:

$$\mu_r = 1 + \chi_m \quad (9)$$

Commercial magnetically soft materials are usually made from alloys of iron and nickel with compositions around Ni₈₀Fe₂₀. Commercial materials have names like 'Permalloy', 'Hymu' and 'Mumetal' and are characterized by high initial permeability and narrow, square hysteresis loops. Myers quotes typical values of remanence at 0.8 times saturation and coercivity about 2 μ T. [Arnold, 2003]

Table 1.2. Some Famous Industrial Materials and Their Parameters

Material	Remarks	Composition	μ	μ_{\max}	Hc (A/m)
Iron	Commercial	99 Fe	200	6000	7.2
Iron	Pure	99.9 Fe	25000	350000	0.08
Fe-Si		96Fe-4Si	1200	6500	40
Fe-Si	GO (Hypersile)	97Fe-3Si	9000	40000	12
50 Permalloy	Hypernik	50Ni-50Fe	4000	100000	4
Supermalloy		79Ni-15Fe-5Mo- 0.5Mn	90000	10 ⁶	0.32
Perminvar	Annealed in magnetic field	43Ni-34Fe-23Co		400000	2.4
Fe-Si-Al	Sendust in powder	85Fe-9.5Si-5.5Al	35000	120000	0.16

Applications of soft ferromagnetic materials are almost exclusively associated with electrical circuits in which the magnetic material is used to amplify the flux generated by the electric currents. Important applications of soft magnetic materials include:

1. inductors and inductive components, low- and high-frequency transformers;
2. AC machines, motors and generators;
3. converters;
4. flexible electromagnetic shielding;

5. magnetic lenses for particle beams and magnetic amplifiers;
6. high-frequency inductors and absorbers;
7. magnetocaloric materials;
8. magnetic and magneto mechanical sensors.

For DC applications: high permeability is required. For AC applications: small energy loss is required. So, Soft Magnetic material produces less heat and easily can magnetized and demagnetized as B-H loop, and small hysteresis loop is good for transformer core and rotating armatures.

A disturbance in alignment of the domains of a ferromagnetic material causes energy to be expended in taking it through a cycle magnetization. This energy appears as heat in the specimen & is called hysteresis loss.

1.5. Soft Magnetic Core:

A magnetic core is a piece of magnetic material with a high magnetic permeability used to confine and guide magnetic fields in electrical, electromechanical and magnetic devices such,as electromagnets, transformers, electric-motors, generators, inductors, the magnetic recording heads, and magnetic assemblies. It is made of ferromagnetic metal such as iron, or ferrimagnetic compounds such as ferrites. The high permeability, relative to the surrounding air, causes the magnetic field lines to be concentrated in the core material. The magnetic field is often created by a current-carrying coil of wire around the core. The use of a magnetic core can increase the strength of magnetic field in an electromagnetic coil by a factor of several hundred times what it would be without the core. However, magnetic cores have side effects which must be taken into account. In alternating current (AC)

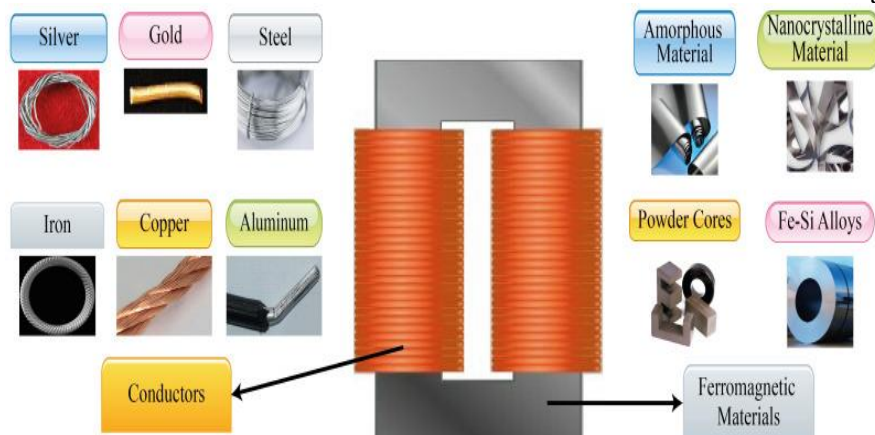


Figure 1.5.: A typical picture of magnetic core source:
<https://doi.org/10.3390/mi13030418>

devices they cause energy losses, called core losses, due to hysteresis and eddy currents in applications such as transformers and inductors. "Soft" magnetic materials with low coercivity and hysteresis, such as silicon steel, or ferrite, are usually used in cores.

1.6 Core Losses:

To any magnetic component designer, a real challenge to overcome is getting a magnetic component with high efficiency, small size, low cost, convenience, and low losses [Lidow A, 2021] Usually, losses are the common factor in all requirements announced before; losses are the most difficult challenges to beat in a magnetic component. Losses in a magnetic component are divided in two groups: core losses and winding losses (also called copper losses), [Jafari et al., 2019]. [Figure 1.6] shows each one of them, as well as their causing phenomena, methods, models, techniques and elements associated with them; nonetheless, phenomena such as the fringing effect and the flux linkage many times are not considered in the losses model. Still, they are necessary to achieve a complete losses model in any magnetic component

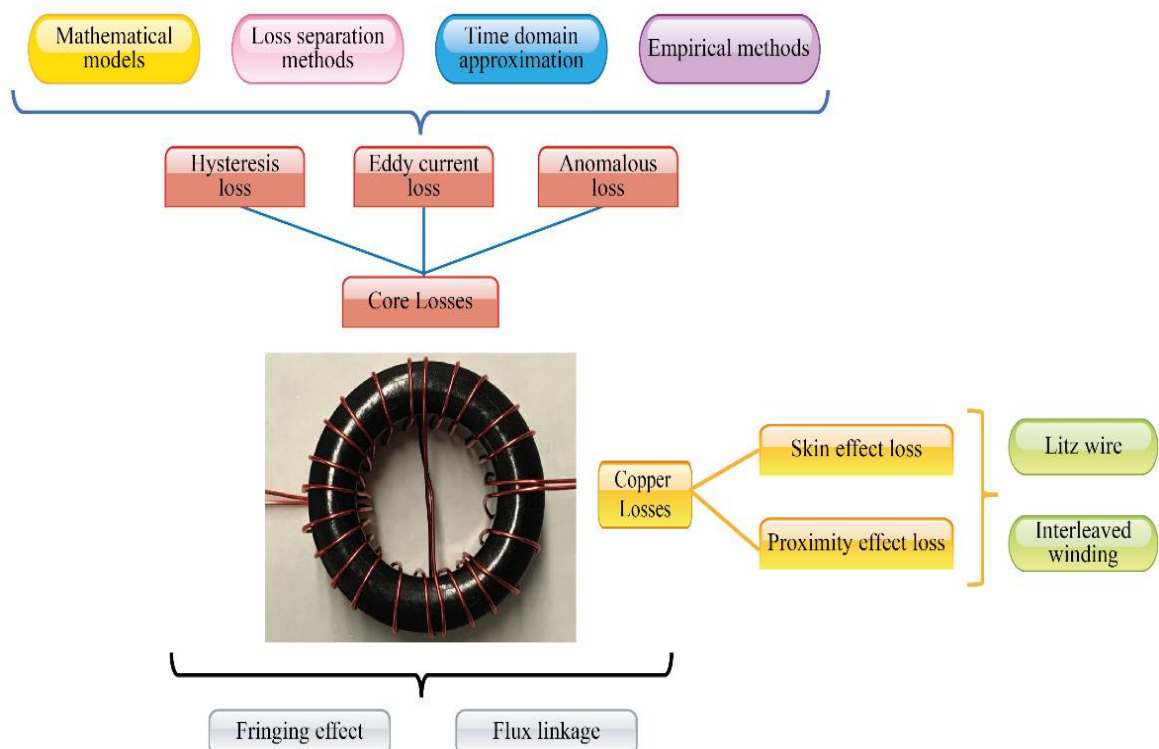


Figure.1.6: Types and classification of losses presented on magnetic components;

Source- (<https://en.wikipedia.org>)

On the other hand, core losses directly depend on the intrinsic and extrinsic core materials' characteristics. Core losses are related to hysteresis loop, Eddy currents, and anomalous or residual losses. Without matter, the core losses model chosen by the magnetic component designer will be based on those three primary losses; core loss models will be detailed in the next section. Besides, core losses depend on the core's geometry and the core intrinsic properties' such as permeability, flux density, Curie temperature, among others [Brighenti and Martins, 2019] [Rodriguez-et al., 2020] [Detka and Górecki. 2020]. Many methods and models have been developed; all of them have the predominant interest in studying, analyzing and understanding those kinds of losses to improve the magnetic components' performance, the average power loss per unit volume P of any material is decomposed into the sum of a hysteresis and a dynamic contribution, which are separately investigated

$$P = P^{hys} + p^{dyn} \quad (10)$$

Frequency Dependence of Losses:

All the irreversible energies utilized in the magnetization and demagnetization process during hysteresis measurements are termed as losses. The total losses depend not only on the type of magnetic material used in the core, but also upon the maximal induction and magnetization frequency. Conventionally total core losses in a soft magnetic metallic material are divided into, hysteresis loss or static loss (P_h), classical loss (dynamic) or eddy current loss (P_{ex}) and anomalous losses (P_a) or excess losses [Bertotti, 1998]

1.6.1 Hysteresis losses

$p^{(hyst)}$ equal to the area of the quasi-static hysteresis loop times f_m . The physical reason for such a decomposition is that $p^{(hyst)}$ originates from the discontinuous character of the magnetization process at a very microscopic scale, whereas $p^{(dyn)}$ is associated with the macroscopic large-scale behavior of the magnetic domain structure. In fact, a proper statistical treatment of the loss problem [Bertotti, 1983], [Bertotti, 1984] shows that (1) is naturally obtained whenever the characteristic time scales of these two processes do not overlap. The material compositions, grain size, grain boundaries, mechanical strains, dislocations and impurities all play a part in domain wall movement and hence in hysteresis losses.

Steinmetz empirically expressed hysteresis loss for normally sinusoidal flux wave $B(t)$ form with varying frequency [Brittain, 1984], nevertheless in case of major loops hysteresis loss depends on the maximum value of the flux density, B_{max} irrespective to magnetic waveform.

$$P_h = k_h f B_{max}^n \quad (11)$$

The parameters k_h are material dependent and can be determined by fitting the experimental data. Steinmetz exponent n range from 1.5 to 2 [Bertotti, 1998], but for most of soft magnetic materials (Fe 3 wt%Si) its value is 1.6 [Bozorth, 1951] The dependence of P_h on B_{max} is predicted by the theory of magnetic domains.

1.6.2 Eddy Current Losses:

The origin of the classical losses in the material are eddy currents due to an alternating magnetic (AC) field produced by an excitation current in the primary windings (according to Lenz's law). The magnetic flux generated by the induced currents opposes the flux changes $\Phi(t)$ produced by excitation current in the core, thus preventing the flux from penetrating the core. The eddy current in general is unfavorable because it weakens the flux inhomogeneous and heats the material [Boglietti et al.,2003]. The induced current is proportional to the rate of change of the induction B , with time (dB/dt). These losses arise from the fact that the core itself is composed of conducting material, so that the voltage induced in it by the varying flux produces circulating currents in the material. These are called eddy currents and are accompanied by loss in the core called eddy current loss. Since the eddy current loss depends upon the rate of change of flux as well as the resistance of the path, it is reasonable to expect this loss to vary as the square of both the maximum flux density and frequency [Fuchs, et al.,2000] simply Eddy current loss is a result of current flows circulating in the core, which is caused by the emf induced from the magnetizing flux for a transformer under normal operating conditions, the primary winding is energized by an alternating current source. A fluctuating magnetic field is produced. An eddy current is induced inside a metal by the varying magnetic field inside the material. This eddy current creates an internal magnetic field opposing the excitation magnetic field. This gives rise to skin effect in which the current density near the outside of the conductor is greater than the inside. Hence the eddy current flows in a ring around the outside of the conducting material.

For each value of the average magnetization rate, the magnetization process in a given cross section of the magnetic lamination can be described, as anticipated in the introduction, in terms of f_j simultaneously active magnetic objects. The dynamic behavior of a single MO is controlled by an equation of the form Hysteresis, where $H_{exc} = p(e')$ is the excess dynamic field acting on the is the magnetic flux rate of change correspondingly provided by the MO, and the proportionality constant determined by the damping effect of eddy currents [Williams et al., 1950].

According to domain wall model the eddy current from adjacent moving domain walls tends to cancel. So, the total losses for the sample are not simply the sum of the losses for each moving

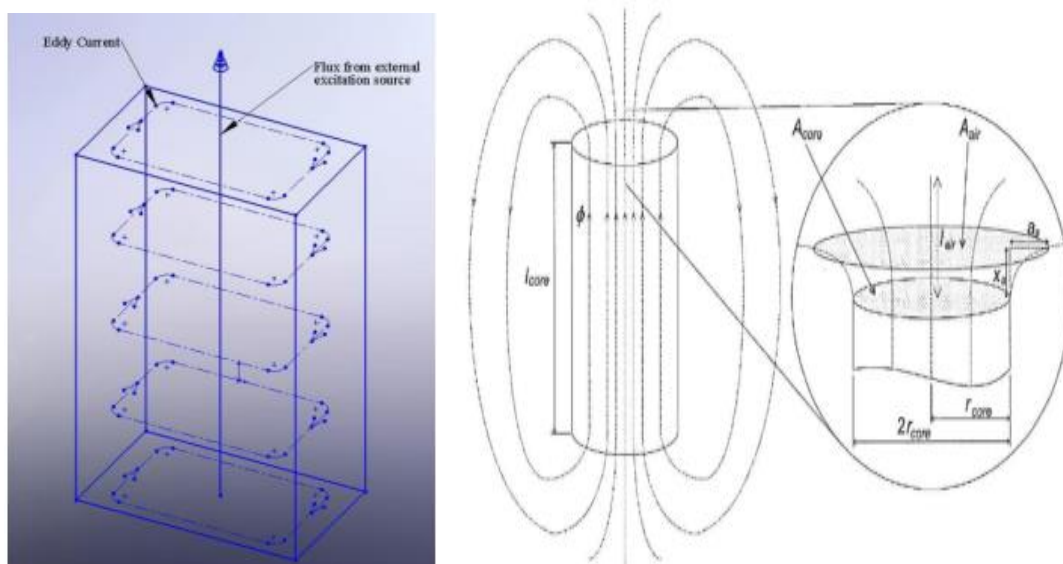


Figure1.6.2 (i): Eddy currents inside a metal block. Flux view of the partial core [Ting, 2009]

domain wall considered independently. The loss for a single moving wall in an infinite medium was first calculated, and loss for a simple array of walls was calculated in a justly celebrated paper Pry & Been. The figure indicates the eddy current flow in a block when there is an external flux passing through it. While the eddy current is depicted as a number of circulating loops in the figure, in actuality, the eddy current is evenly distributed over the entire length of the metal in the direction of the flux. [Ting, 2009] The domain walls need not remain planar, as assailed in the simplest model. A 180 wall may develop

curvature about an axis parallel to the easy direction «without an increase in magnetostatic energy. The shielding effect of eddy currents can cause the field at the surface to exceed that at the center of the sample sheet, and consequently cause the domain wall at the surface to move ahead of the center portion of the wall. The phenomenon is known as domain wall bowing. A moving bowed wall spreads the eddy-current loss over a larger volume than a "moving plane wall", and so reduces the losses slightly. However, the direction of the bowing reverses when the direction of wall motion reverses; this means that the magnetization reversal is to some extent concentrated in the surface layer and this increases the eddy-current loss [Graham, 1982]. The eddy current losses can be reduced, by increasing the resistivity of the material. Since ferrites have a high resistivity, eddy currents are small until higher frequencies are encountered [Goldman, 2006].

The classical eddy current loss was described by the Steinmetz law,

$$p_{ex} = K_{ex} f^2 B_{\max}^2 (J/m^3) \quad (12)$$

According to the statistical theory described by Bertotti and Fiorillo the expression for calculating the classical eddy currents losses:

$$P_{ex} = \Pi^2 d^2 f^2 B_{\max}^2 \rho \beta (J / m^3) \quad (13)$$

Where d is thickness of the lamination, ρ is the electrical resistivity of the material and β is a constant which depends on the shape of driving field.

Way To Control Eddy Current Loss-

1. The core's resistance should be increased.
2. A thin layer of varnish should be used to insulate the thin sheets of steel in the core of transformers. Because the laminations are thin, they will be relatively resistant
3. The planes of these sheets are perpendicular to the direction of the current created by the induced emf.
4. These sheets' planes are arranged parallel to the magnetic fields in order to cut across the eddy current paths.

Eddy currents are limited to thin sheets due to the high resistances between them. An eddy current will circulate within each lamination sheet. Tiny eddy currents still exist, but they are much reduced because they exist only within each thin sheet.

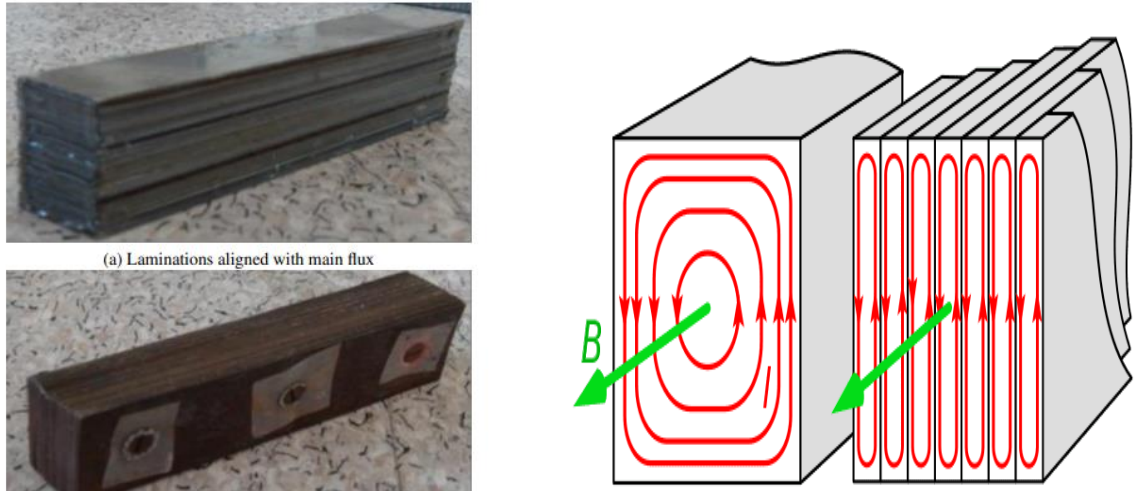


Figure 1.6.2(ii): Two rectangular billets with different lamination orientations [Ting, 2009]

1.6.3 Anomalous or Excess Losses:

The important conceptual simplification introduced by the separation of losses is readily appreciated, because the interpretation of $p^{(dyn)}$ —the quantity of principal interest in this paper—can then be based on simple macroscopic domain models, paying no heed to the intricate fine-scale details of wall motion. In this connection, the so-called "classical" model [Graham, Jr, 1982] [Bozarth, 1951] even disregards the very presence of magnetic domains and assumes a magnetization process perfectly homogeneous in space. In the case of a lamination of thickness d and in the range of magnetizing frequencies where the skin effect is negligible, this model predicts (sinusoidal flux waveform)

$$P_{dyn} = P_{class} = \pi^2 \sigma d^2 I^2 f_m^2 / 6 \quad (14)$$

where σ is the electrical conductivity of the material. The classical model is, however, too gross a simplification. As a consequence of domain effects, the dynamic loss $p^{(dyn)}$ is generally found to be definitely larger than $p^{(class)}$, the difference between them, called excess loss $p^{(exc)}$, being in many cases larger than $p^{(class)}$ itself. By expressing the total loss as

$$P_{total} = P_{hys} + P_{class} + P_{exc} \quad (15)$$

$$P_{exc} = P_{total} - P_{hys} - P_{class} \quad (16)$$

Loss Separation Models

The loss separation method (LSM) is well-known, accurate and straightforward in many applications [Ducharne et al., 2021]. It defines the core loss (PC) under a dynamic magnetic excitation as the sum of three components: the hysteresis loss (P_h), the Eddy current loss (P_{eddy}) and the residual or anomalous loss (P_{anom}) [Dong et al., 1995] is given by the above equation. Years later, Bertotti extended Jordan's proposal, adding an extra term to calculate residual losses. G. Bertotti is the maximum exponent in the loss separation methods; his theory provides a solid physical background. The total power loss can be calculated at any magnetizing frequency as the sum of three components [Appino et al., 2016]. This is shown in the following equation

$$P_{total} = k_h f B_x + K_{eddy} f^2 B^2 + K_{anom} f^{1.5} B^{1.5} \quad (17)$$

where k^h , k^{eddy} , k^{anom} are the hysteresis, Eddy currents, and anomalous coefficients, respectively. The hysteresis coefficient decreases if the magnetic permeability increases. The frequency is represented by f , while x is the Steinmetz coefficient and has values between 1.5 and 2.5, according to the permeability of the material. Finally, B_s is the peak value of the flux density amplitude [Balci and Sefa, 2014; Bertotti, 1988]. From Equation (17), Bertotti defined eddy currents and anomalous losses in Equations (18) and (19), respectively, for lamination materials.

$$P_{eddy} = \pi^2 \sigma d^2 I^2 f_m^2 / 6 \quad (18)$$

$$P_{exc} = C B_{max}^{1.5} \sqrt{f} = 8 \sqrt{\frac{G A V_0}{\rho}} B_m^{1.5} \sqrt{f} \quad (19)$$

where G is about 0.2, ρ is the electrical resistivity, d is the lamination thickness, A is the cross-sectional area of the lamination, β is the magnetic induction exponent, G is a dimensionless coefficient of Eddy current, and V_0 is a parameter that characterizes the statistical distribution of the magnetic objects responsible for the anomalous eddy currents [Mehboob, 2012]. However, this method only provides average information, so it is not able to calculate core loss under harmonic excitation [Ducharne, 2021]. Still, it can calculate core loss under square waveforms considering DC bias [Sun et al., 2020].

Where A is the cross-sectional area of the lamination, G is a dimensionless coefficient of the eddy current damping which is about 0.2 and ρ is electrical resistivity. V_0 is a parameter

characterizes the statistical distribution of the magnetic objects responsible for the anomalous eddy current

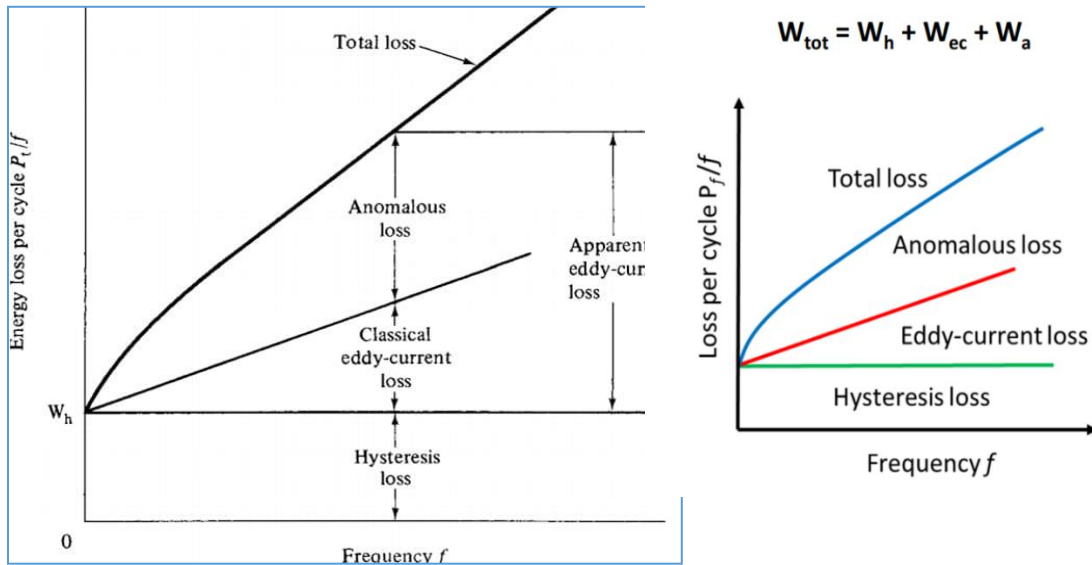


Figure:1.6.3 No- Load loss into Its Component, [Takach.D.S., Boggavarapu.R.L.,1985]

Table 1.3: Some Famous Industrial Material Core Loss

Material	Core Loss at 1.5 T and 60 Hz (W/kg) Low-carbon steel
Low-carbon steel	2.8
Non oriented silicon-iron	0.9
Grain-oriented silicon-iron	0.3
80 Permalloy (Ni80Fe20)	0.2

CHAPTER 2: LITERATURE REVIEW

2. Literature Review

Metal soft magnetic material is one of the most widely used magnetic material. The frequently used metal soft magnetic material includes pure iron, silicon steel and permalloy. The application of metal soft magnetic material in the industry has a history of more than one hundred years and its development can be divided into four stages. The period before 1930s can be generally regarded as the first stage in the development of metal soft magnetic material. Since the 1800s, when iron was the only soft magnetic material available and with the emergence of the electric power industry and telecommunication engineering, low-carbon steel began to produce transformer and motor at end of 19th century. Replacing steel by silicon steel effectively reduced loss at the beginning of the 20th century and silicon steel still ranks first for soft magnet demand in power industry up to now. Meanwhile, weak current engineering laid down high permeability requirement for material with the progress of telephony, then an array of soft magnetic alloys emerged as the times require. By the 1920s, the rise of radio technology further promoted the development of high permeability soft magnetic alloy, then permalloy, mu-metal, perminal alloy, hiperco alloy and permalloy powder core appeared. Metal soft magnetic material experienced the second stage of development between 1930s and 1940s, then its variety, magnetic properties and application have been developed rapidly during this period. The representative achievements include multi-element permalloy, Fe-Si-Al high permeability alloy and unidirectional silicon steel. Meanwhile, researchers found that magnetic heat treatment and rolling can establish induced anisotropy in the permalloy and studied ordered lattice structure in the permalloy and iron-cobalt alloy. In addition, magnetic physics have also made considerable headway such as proposed spin-wave theory and the energy band theory of ferromagnetism; magnetic domain and structural theory of domain wall; coercivity theory and technical magnetization theory; and mechanism of magnetic loss. Metal soft magnetic materials underwent the third process of development between 1940s and 1970s. Adventure and development of emerging technology put forward higher request to magnetoelectric properties of metal soft magnetic material, especially electronic technology and instruments. Representative materials in this period include high rectangular hysteresis loop alloy, high permeability alloy, magnetic thin film, soft magnetic alloy strip and doubly oriented silicon steel. Furthermore, researchers measured magneto crystalline anisotropy constant and saturation

magnetostriction constant of various soft magnetic alloys, studied the origin of high permeability and clarified the mechanism of magnetic heat treatment. Since 1970s, the development of metal soft magnetic materials entered into the fourth stage. Besides high efficiency, high stability and durability, metal soft magnet is required to possess a low cost. Researchers studied the relationship between magnetic performance and various factors in metallurgy, and change rule between material properties and various external conditions.

However, its low electrical resistance makes it subject to large losses from eddy currents, particularly as operating frequencies are increased. This leaves the soft magnetic community looking to other materials to meet the needs of newer high frequency devices.

Ever since Michael Faraday demonstrated electromagnetic induction in 1831, there has been a continuing evolution of soft magnetic materials. Faraday's natural choice of core material was iron, which has the highest room temperature M_s of any element in addition to a large t_i and fairly low H_c . However, even in a simple material comprised of a single element there was room for considerable improvement. It was discovered that annealing iron not only improved its mechanical properties but also decreased its coercivity through stress relief, making it better suited for use in inductive applications.

Seeking even better performance, scientists and engineers looked for ways to improve upon the properties of soft iron.

In 1900, Robert Hadfield, a metallurgist from England, invented non oriented silicon steel by adding up to 3% silicon to iron and increasing its electrical resistivity (ρ) while also increasing μ_r , [Cullity and Graham, 2009]. American metallurgist Norman Goss invented grain-oriented silicon steel in 1933 by promoting grain growth along a crystalline direction of low anisotropy, increasing (μ_r),, even further [Cullity and Graham, 2009]. Even today, silicon (or electrical) steels account for a major share of the global soft magnet market because of their high M_s and relatively low cost [Appino et al., 2016]. The most common applications for silicon steel are large-scale transformers (grain-oriented silicon steel) and electrical machines (isotropic non oriented silicon steel is preferred for rotating machines), where its economical price is a huge benefit. However, a low (ρ) (-, 0.5 m ohm.m) ["Super CoreTM JFE Steel Corporation, 2017] makes silicon steels lossy at high frequency. Recently, electrical steel manufacturers have developed a path to increase the silicon content of their steel to 6.5% using a chemical vapor deposition (CVD) process [Shoji et al.,2016].

This approach increases p to 0.82 (μ_r), Q.m but still leaves other materials as better choices for high-frequency power electronics and high rotational speed electrical machines.

In the 1910s, Gustav Elmen at Bell Laboratories experimented with nickel-iron alloys and discovered the nickel-rich (78%) permalloy composition [Arnold and Elmen,1923]. A major advantage of permalloy is its high (μ_r). (Up to 100,000). Nickel-iron alloys are still used in some specialty inductive applications today but are not common in power electronics and electrical machines because they have high eddy current losses, and the addition of nickel decreases M . With the addition of a small amount of molybdenum (2%) to permalloy, moly permalloy powder (MPP) can be produced [Alabakhshizadeh and Midtgård , 2013]. MPP is used to fabricate the lowest loss powder cores [Alabakhshizadeh and Midtgård, 2013]. which will be discussed in more detail below.

In the late 1940s magnetically, soft ferrites were invented by J. L. Snoek [De Vries, (1914-1994).]. These materials are competitive because of their very high electrical resistivities (10 - 108 (ρ). ohm.m), which make them effective at suppressing eddy current losses. Additionally, because they are produced with ceramic processing techniques and abundant materials, ferrite parts can be produced at a very low cost. The high p and affordability of soft ferrites keeps these materials in high demand for inductive applications, including those at high frequency. In fact, their share of the global market in soft magnets is second only to silicon steel [Cullity and Graham, 2009]. They do suffer from a relatively low M_s (nearly a quarter of that of silicon steel), which limits the energy density of inductive elements containing a ferrite core.

In 1967, Duwez and Liz reported the first amorphous soft magnetic alloy in the form of small disk-shaped samples. They used a rapid solidification technique called splat cooling for the Fe-P-C system [Duwez, 1967]. Alloy composition engineering and the development of planar flow casting led to the production of amorphous ribbons from 5 to 50 gm in thickness and up to 10 inches (25.4 cm) in width (. By the mid-1970s, interest in iron and cobalt based amorphous alloys was surging and they began finding their way into applications. Through the elimination of any long-range order, coercivity is substantially reduced in these alloys.

In 1988, researchers at Hitachi included Nb and Cu additives and added an annealing step to the production of amorphous alloys to produce small and closely spaced crystallites of iron or cobalt (on the order of 10 nm in diameter) within a matrix of amorphous material [Yoshizawa et al., 1988]. This was the inception of the nanocrystalline soft magnetic alloys. The formation of isolated transition metal crystallites reduced the eddy current losses of these materials in comparison to amorphous alloys. Both amorphous and nanocrystalline alloys are gaining market share in high-frequency power electronics and electrical machines today because of their low losses and competitive M. Despite a higher initial cost than silicon steel, these advanced alloys can reduce the total lifetime costs of power electronics and electrical machines, thanks to reduced losses.

In the early 1990s, powder cores (also known as soft magnetic composites or SMCs) gained acceptance in some soft magnetic applications [Cullity and Graham, 2009] [Yoshizawa et al., 1988]. These materials combine magnetic particles, anywhere between approximately 1 to 500 nm in diameter, and either coat or mix them with an insulating material before consolidating with high pressures (MPa to even GPa pressures). Heat can also be applied either during or after densification to improve magnetic properties. The magnetic particles are most often Fe powders but can also consist of alloys such as MPP (mentioned earlier), Fe—P, Fe—Si, or Fe—Co. Because of the insulating and non-magnetic matrix phase, these materials have a distributed air gap that limits their μ_r to a range of 100 to 500. However, the insulating matrix also boosts their ρ (10^{-3} to 10^{-1} $\mu\text{ohm}\cdot\text{m}$), reducing eddy current losses. SMCs can also be pressed into more complex final geometries without the need of any machining (net-shaping), which can substantially reduce manufacturing costs. Their isotropic nature, low cost, and the ability to net-shape complex parts have made SMCs fairly successful in rotating electrical machines [Jack et al., 2000] [Hultman and Jack, 2003].

In early 2000, McHenry Developments in the of magnetic materials which show promise for future applications are reviewed. In particular recent work in nanocrystalline materials is reviewed, with either soft or hard behavior as well as advances in the magnetic materials used for magnetic recording. The role of microstructure on the extrinsic magnetic properties of the materials is stressed and it is emphasized how careful control of the microstructure has played an important role in their improvement. Important microstructural features

such as grain size, grain shape and crystallographic texture all are major contributors to the properties of the materials. In addition, the critical role that new instrumentation has played in the better understanding of the nano-phase magnetic materials is demonstrated. [McHenry, 2000]

Furthermore to make more efficient soft magnetic alloy Janghorbah in 2007 has reported in the general of materials processing technology He showed that SMC can be described as ferromagnetic powder particles surrounded by an electrical insulating film so, that 3d isotropic ferromagnetic behaviors, very low eddy current loss ,relatively low total core loss at medium and high frequencies for improved thermal characteristics ,flexible machine design and assembly a prospect for greatly reduced weight and production cost.

The brief history of soft magnetic materials described above is by no means exhaustive. Instead, our intent is to focus on materials that have been and will continue to be competitive for the fabrication of soft magnetic components in high-frequency power electronics and electrical machines. Performance metrics such as M_s and core loss are extremely important. However, because soft magnetic parts will need to be used in large quantities, the importance of cost cannot be neglected. For this reason, soft ferrites still remain a competitive core material at high frequency. Because of their excellent performance at high frequency, the amorphous and nanocrystalline alloys will certainly continue to be key materials. Although silicon steels still make up a majority of the global market for soft magnetic materials, their primary applications are in large transformers operating at 50 or 60 Hz and slow rotational speed electrical machines. Thus, we will not discuss silicon steel further. We will also consider new soft magnetic materials being developed, which include both top down and bottom-up approaches that could build upon a foundation of work established in the area of SMCs.

CHAPTER 3: AIMS AND OBJECTIVE

2.1 Aims of this project

There are numbers of loss separation model in the literature to analyze the losses in magnetic core materials. However, every model has its shown merits and demerits. Separation of losses from the overall core loss is very tricky and laborious job. Moreover, there is no universally accepted loss separation model, which can be applicable for all types of core materials. Therefore, the main aim of this project work is to select a suitable model and use it for analyze the core losses in presently studied sample (Fe-P-Si ferromagnetic alloy). A new model which has a physical basis for the variation of loss coefficients with alternating flux density and/or frequency has been developed by Lotten [Mthombeni, 2006] using the laboratory test bench results. The purpose of this thesis is to examine the applicability and accuracy of the new model using the recent core loss results from the new testing equipment and frames. The model is tested in induction and permanent magnet synchronous machines. Therefore, the aim of this project work is-

“Provide a contribution to understanding magnetization losses in soft metallic ferromagnetic material that may be useful for both physicist and engineering section.

2.2 Objectives of this project

The prime objective of this thesis is to characterize the soft magnetic alloy at high frequencies and high flux densities using the new Epstein frame. Further, to compare the Epstein, Toroid and Single Sheet Tester (SST) core loss test frames in order to determine their impact on core loss measurement and modeling. The objectives of this thesis work are-

- a) Basically, we shall examine the dependence of power losses on magnetizing frequency, f from 0 to 20 kHz and peak magnetic flux density, B up to 1.25 Tesla. We tried to clarify how these properties depend on the parameters like grain size that define the micro structural of a given material as like domain size that characterized its magnetic domain structure.
- b) We want to reduce the magnetic core loss to maximize the efficiency of the soft magnetic material in use machinery like transformer, motor engines, electronic circuits etc.

- c) To investigate and understand the losses associated with soft magnetic materials when subjected to an alternating current (AC) magnetic field.
- d) To analyze the factors influencing the losses in soft magnetic materials under AC conditions.
- e) To identify the various mechanisms contributing to losses in soft magnetic materials in AC fields.
- f) To develop strategies for minimizing losses in soft magnetic materials used in AC applications.
- g) To enhance the overall efficiency and performance of devices utilizing soft magnetic materials in AC circuits.

CHAPTER 4: MATERIALS AND METHODS

4. Materials and Methods

In a magnetic component, the core is the key to determine its magnetic properties and performance [Jiandong et al., 2018] So to achieve an optimal magnetic component's performance, the core losses effects must be characterized [Saeed et al., 2020]. Core loss depends on many aspects that must be considered [Ishikura et al., 2018]:

- Relative permeability.
- Magnetic saturation point.
- Temperature operation range.
- AC excitation frequency and amplitude.
- Voltages' waveform.
- DC bias.
- Magnetization process.
- Peak-to-peak value of magnetic flux density.

In the case of the magnetization process, some factors are instantaneous values and time variation values. While to waveform's topic, the duty ratio of the excitation waveform also influences the core loss [Yue et al., 2018].

Generally, the core loss is provided at a specific frequency and a maximum flux density. The variation frequency effect in ferromagnetic materials is related to Eddy currents and the wall-domain displacement [Jiandong et al., 2018].

Core losses in ferrimagnetic and ferromagnetic materials are similar. Both have losses due to Eddy currents, hysteresis, and anomalous; however, there are differences concerning flux density, magnetization process, and hysteresis loop shape that define the magnetic behavior of each one.

The hysteresis is one of the principal features of ferromagnetic materials; it describes the internal magnetization of magnetic components as a function of external magnetizing force and magnetization history [Wiley, 2012]. The source of hysteresis loss is the domain wall movement and the magnetic domains' reorientations [Wiley, 2012]. The hysteresis loss is

defined as power loss in each cycle of magnetization and demagnetization into a ferromagnetic material [Dong et al., 1995]. If a magnetic sample is excited from zero to the maximum field value and later comes back at the initial field's value, it will be observed that the power returned is lower than the supplied it. The loss is proportional to the area surrounded by the upper and lower traces of the hysteresis curve; it represents the per cycle loss and it is proportional to $f \cdot B^2$ [Dong et al., 1995]. However, if the curve's shape remains equal for each successive excitation, the loss power will be the product of the core's area and the applied frequency [Dong et al., 1995].

The hysteresis loops give a lot of information about the magnetic properties [Yue et al., 2018]. An accurate way to calculate core loss is by measuring the full hysteresis curve.

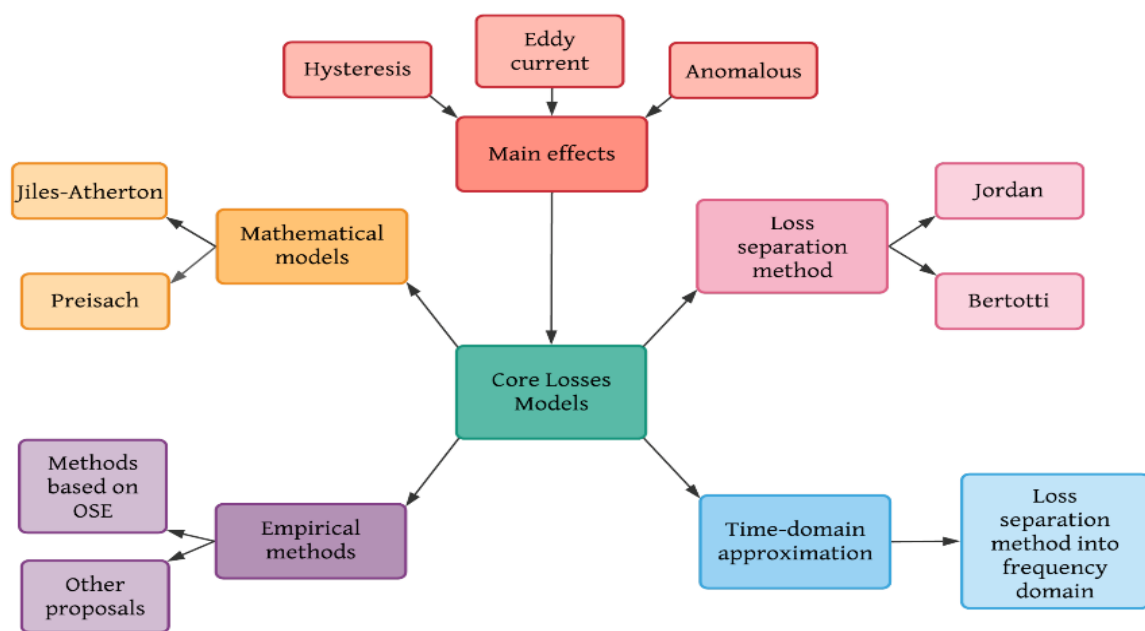


Figure 4: Different core loss model for calculate loss separation in magnetic core,
Source- (<https://en.wikipedia.org>)

4.1 Mathematical Models

Mathematical hysteresis modelling is divided into approaches based on the theory of micro-magnetics and the methods based on curve-fitting. The hysteresis models require complex computation to calculate the model parameters, the material parameter that manufacturers do not provide, or mathematical approximations where the accuracy depends on the number

of data points to fit hysteresis loops [Ram and Kulkarni, 2019]. These drawbacks remain if they are analyzed from a purely mathematical or a physical point of view.

The Preisach model and the Jiles-Atherton (J-A) model have been widely used in practical problems to calculate core loss, they are in continuous improvement, and they are considered a valuable and convenient tool to the hysteresis modelling [Zhao et al., 2019].

The Preisach is a scalar-static model that considers several quantities of basic's domain-walls [Jiandong et al., 2018]. It is an accurate-phenomenological model, such that it could describe any system that shows a hysterical behavior. This model can be a link between theory and experimentation to describe a microscopical system by measuring macroscopic behavior.

4.2 Loss Separation Models

The loss separation method (LSM) is well-known, accurate and straightforward in many applications [Ducharne et al., 2021]. It defines the core loss (PC) under a dynamic magnetic excitation as the sum of three components: the hysteresis loss (P_h), the Eddy current loss (P_{eddy}) and the residual or anomalous loss (P_{anom}) [Dong et al., 1995] is given by the above equation Years later, Bertotti extended Jordan's proposal, adding an extra term to calculate residual losses. G. Bertotti is the maximum exponent in the loss separation methods; his theory provides a solid physical background. The total power loss can be calculated at any magnetizing frequency as the sum of three components [Appino et al., 2016]. This is shown in the following equation (17) where k^h , k^c , k^{anom} are the hysteresis, Eddy currents, and anomalous coefficients, respectively. The hysteresis coefficient decreases if the magnetic permeability increases. The frequency is represented by f , while x is the Steinmetz coefficient and has values between 1.5 and 2.5, according to the permeability of the material. Finally, B_s is the peak value of the flux density amplitude [Balci and Sefa, 2014] [Bertotti, 1988]. From Equation (17), Bertotti defined eddy currents and anomalous losses in Equations (18) and (19), respectively, for lamination materials. where G is about 0.2, ρ is the electrical resistivity, d is the lamination thickness, A is the cross-sectional area of the lamination, β is the magnetic induction exponent, G is a dimensionless coefficient of Eddy current, and V_0 is a parameter that characterizes the statistical distribution of the magnetic

objects responsible for the anomalous eddy currents [Mehboob,2012]. However, this method only provides average information, so it is not able to calculate core loss under harmonic excitation [Ducharme,2021]. Still, it can calculate core loss under square waveforms considering DC bias [Sun et al.,2020].

4.3. Empirical Models:

A big group of empirical models is based on a simple power-law equation, which was proposed in 1982 by Charles Steinmetz to calculate hysteresis loss without including the frequency relation [Steinmetz 1892]. This equation is known as the Steinmetz equation or original Steinmetz equation (OSE)

$$P^{ose} = Kf^{\alpha}B^{\beta} \quad (20)$$

In modern power electronics applications, sinusoidal-wave voltage excitation is not practical because many of them, like power converters, require square-wave voltage excitation. Finally, the Waveform-Coefficient Steinmetz Equation (WcSE) was proposed in [Shen W.et al., 2007] to include the resonant phenomena, and it applies only at situations with certain loss characteristics. This empirical equation is used in high-power, and high-frequency applications, where resonant operations are adopted to reduce switching losses. The WcSE is a simple method that correlates a non-sinusoidal wave with a sinusoidal one with the same peak flux density; the waveform coefficient (FWC) is the ratio between the average value of both types of signals. WcSE can be written as follows:

$$P^{wcse} = FWCKf^{\alpha}B^{\beta} \quad (21)$$

4.4 Core Loss Modeling

Core Loss Modeling In the design of electric machines, predicting core losses has always been a difficult task. Various core loss models have been developed based on the work of Steinmetz [Steinmetz, 1982] The Steinmetz's initial model has been developed based on the phenomenological principle known as loss separation; hence it is composed of two terms, which are the hysteresis and eddy current loss components [Steinmetz, 1982]. The model has been developed by curve fitting the experimental data and is in the form of

$$\bar{P} = k_h B^2 f + \frac{\sigma \pi^2 d^2}{6\rho} B^2 f^2 + k_{ex} B^{1.5} f^{1.5} \quad (22)$$

where k_{ex} is the excess loss constant coefficient, which depend on material intrinsic parameter and dimensions. The model was tested up to 100Hz and was not expected to work for all materials and frequencies [Betrotti,1998]. Since then, many core loss models have been developed and refined. In some models, loss coefficients vary with flux density or frequency or both. The core loss data used are for materials subjected to sinusoidal flux density waveforms. Based on the number of research papers produced, it is clear that mathematically, a large number of core loss models can be developed. Although, good results are obtained from these models, they lack a physical basis to explain the variation of loss coefficients. Most of these models are tested for sinusoidal flux waveform cases only using one or two materials and therefore lack wide representation of the model. To calculate core losses under non-sinusoidal flux densities, the Fourier series technique is used in these models.

4.4 Core Loss Measurement Concept

It has been found as early as 1890's [Manyage and Pillay, 2007] through experiments that when an applied magnetic field H_a is cycled in a magnetic material, energy is converted to heat and sound due to the magnetic hysteresis of the material. The hysteresis phenomenon is best described by a four-quadrant hysteresis loop in [Figure 2.1], also known as the BH loop; where the area inside the loop represents the energy loss per cycle [Betrotti,1998]. Different types of material have different shapes of hysteresis loop but the overall energy per cycle (W.s/cycle) per unit volume, E_{loop} , is given by

$$E = \oint H \cdot dB \quad (23)$$

Therefore, the power loss or core loss in watts per unit volume, P_c , will be

$$p = f \int H dB \quad (24)$$

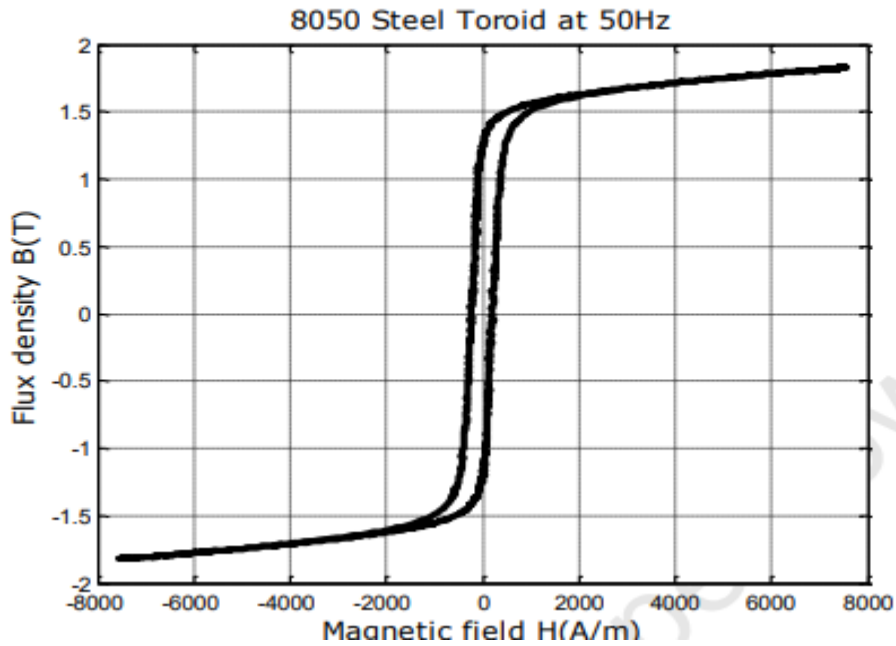


Figure 4.4(i): ac hysteresis loop

where B is the alternating flux density observed over one electrical cycle of frequency f . The core loss formula (25) represents the total loss in a material, that is, it includes hysteresis, eddy current and excess losses [Betrotti,1998]. Therefore, hysteresis losses should not be confused with the hysteresis loop in [Figure 4.4(i)] The loss measurement concept is based on the transformer like electromagnetic circuit shown in [Figure 4.4(ii)]. V_p , I_p , E_p , R_p and L_p are primary voltage, current, back EMF (all in rms), resistance and

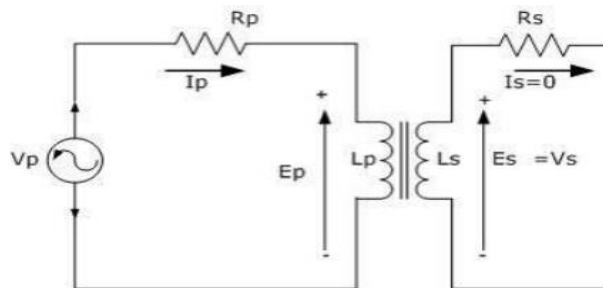


Figure 4.4(ii): Core loss measurement electromagnetic circuit

inductance respectively. E_s , V_s , i_s , R_s and L_s are secondary voltages, current, winding resistance and inductance respectively.

Core Loss Measurement Concept

Two core loss testing equipment are used during the core loss measurement and analysis process. The description, capabilities and comparison of the two systems are given below.

Donart System:

The Donart system in [Figure 4.2(iii)] is the new commercial computerized equipment capable of automatic core loss measurement at low and high flux densities and wide frequency range. It consists of a signal generator, AE Techron amplifier, computer, controller, current/voltage measurement outputs and three test frames (Epstein, Toroid and Single Sheet Tester). The Donart system core loss measurement is based on the ASTM standard, thus adopting the ASTM schematic in Figure 2.4 but with modern instrumentation. Its drive capability is limited at 120V, 15A with a signal generator with

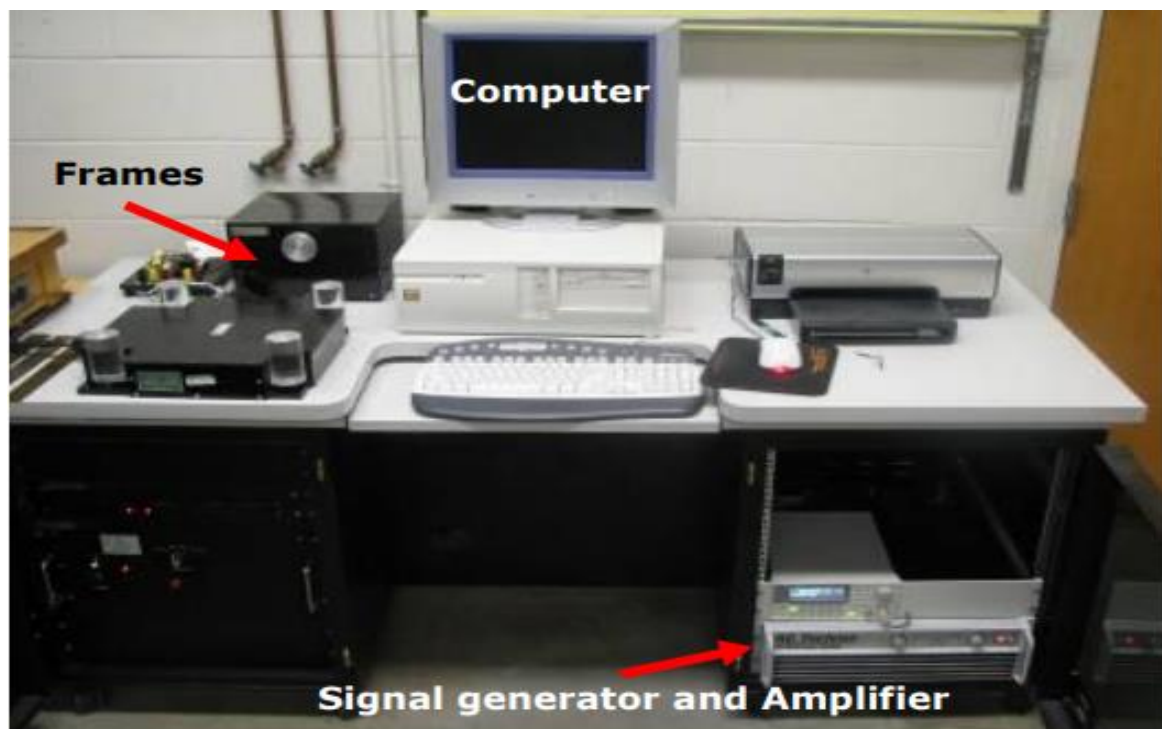


Figure 4.4 (iii): Donart testing equipment

frequency range from 20Hz to 4kHz. AC Hysteresis loops as shown in [Figure 4.1.(i)] are possible from 20Hz to 400Hz

Test Bench System:

The test bench system in [Figure 4. (iv)] is a powerful testing equipment capable of measuring core losses with any arbitrary waveforms and frequencies (within limits). Its control is flexible and allows non-sinusoidal core loss testing thereby surpassing the commercial test systems, which are limited to sinusoidal excitations only. It consists of computer with dSpace board (DS1104), AE Techtron high bandwidth linear amplifier and measuring instruments (DL750 scope and wattmeter). The diagram in Figure 4. (iv) shows the test bench system connection more clearly. Signals are generated in MATLAB\Origin interfaced with dSPACE for real-time control, and applied to the frame under test (Epstein or Toroid).

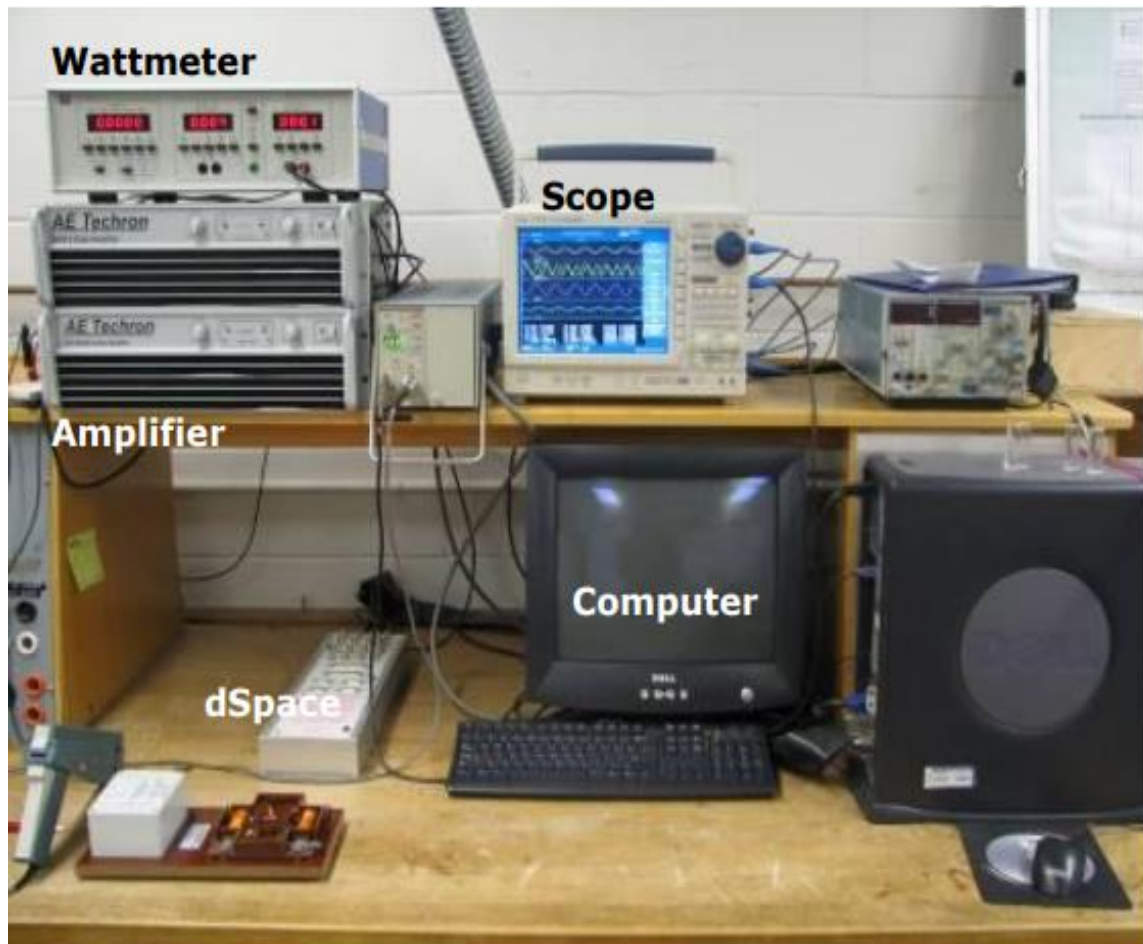


Figure 4. (iv): Test bench testing equipment

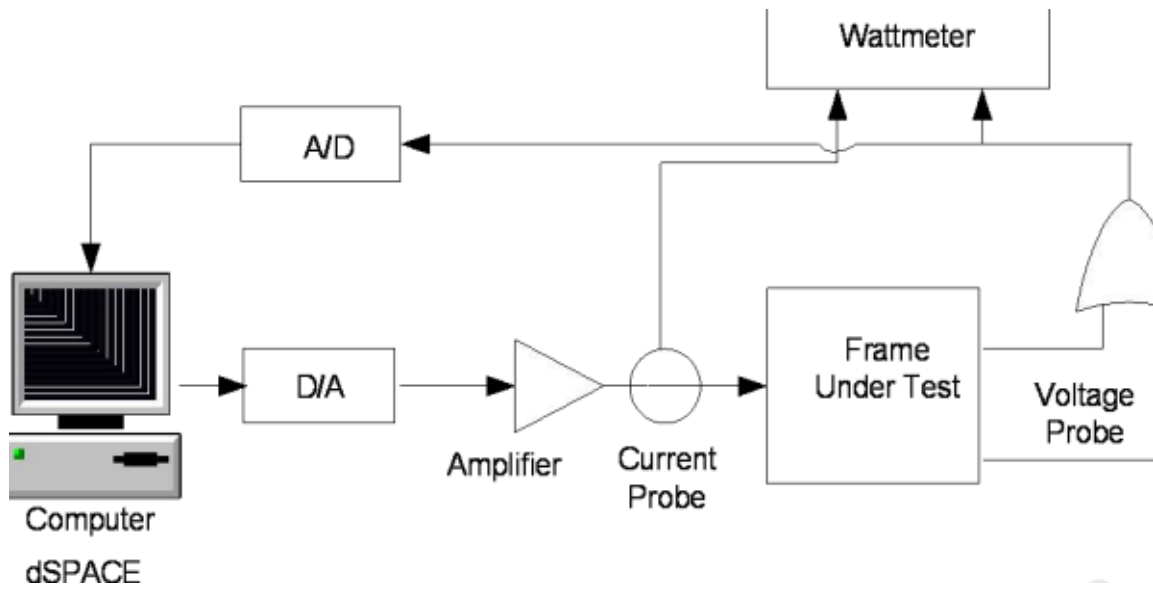


Figure 4.4 (v): Test bench schematic

CHAPTER 5: RESULTS

5.Results

5.1 Study on Frequency dependent coercivity:

The coercivity (H_C) is an important parameter of magnetic materials for defining their role in technical applications. The coercivity of a magnetic material depends upon the domain wall movement, which is greatly influenced by the microstructural changes induced by mechanical and thermal treatments. At quasi static frequencies the increase in coercivity is due to structural defects such as particles of a nonmagnetic phase or voids in the magnetic material tend to restrict the motion of domain walls. An analysis of the frequency dependence of coercivity is helpful in understanding the dynamic coercivity mechanism in soft magnetic materials. There are several possibilities to analyze the frequency dependence of H_C very general

One can assume that H_c scales with some power of frequency (f) which leads to Equation (25)

One can develop $H_C(f)$ into different powers of frequency (26)

$$H_C(f) = a + bf^c \quad (25)$$

$$H_C(f) = d + ef^{0.5} + gf \quad (26)$$

Where parameters a and d in the equations correspond to the coercivity at 0 Hz i.e., $H_C(f=0)$ and b , c , e and g are free fit-parameters. These parameters depend on the microstructure as well as the magnetic field amplitude H_0 and also on $H(t)$. In equation (25) coefficient e described the normal “classical” eddy currents whereas the anomalous eddy current damping represented by g becomes dominant especially at higher external fields.

Zhukov and coworker [Zhukov et al.,2009] analyzed the frequency behavior of the coercivity in amorphous materials with the general formula (26) which was derived for triangular wave form of the field with:

$$H(t) = 4ftH_0 \quad (27)$$

$$H_c(f) = H_c(0) + B.(f.H_0)^{1/n} \quad (28)$$

Where H_0 is the field amplitude and n can vary between 1 and 3 depending on the geometry and on the microstructure of the material as well as on the frequency range considered.

Formula (26) is equivalent with a fit using Equation. (25); with the parameter B corresponding to $b/[H_0]^{1/n}$ which correlates to the dynamic coercivity field.

The term $H_c(0)$ corresponds always to the zero frequency extrapolated which is the “true” coercivity. The power factor c in equation (26) that correspond to a high frequency solution or to the effect that also anomalous eddy current damping of the domain walls occurs as described in [Zhukov et al.,2009] therefore its value should be comparable to n in equation (28).

The experimental data of the frequency dependence of the coercivity at room temperature the fitting results on experimental data are shown in **Figure 5.1** for Fe-P-Si samples respectively. The parameters obtained from the such fitting are given below **Table 5.1(b)**:

Table 5.1(a): Data chart for Frequency dependent coercivity in Fe-P-Si

FREQ. Hz	Hc A/M FePSi (0.45T)	Hc A/M FePSi (0.65T)	Hc A/M FePSi (1T)	Hc A/M FePSi (1.25T)
0	31.05	37.94	42.26	41.85
10	48.73	61.52	74.99	94.71
20	58.11	74.63	93.59	118.37
30	65.67	82.42	103.88	111.76
40	70.34	69.9	106.29	122.25
50	76	95.14	119.18	144.03
70	84.53	98.04	130.17	172.18
100	97.44	115.47	154.54	216.59
150	114.51	141.74	188.93	267.41
200	131.26	168.29	224.88	302.77
250	146.09	196.33	259.63	334.97
300	160.38	214.19	292.41	350.38

350	174.67	232.82	322.74	375.22
FREQ. Hz	Hc A/M FePSi (0.45T)	Hc A/M FePSi (0.65T)	Hc A/M FePSi (1T)	Hc A/M FePSi (1.25T)
400	187.06	250.31	357.54	414.91
450	199.39	268.91	386.72	451.76
500	209.28	286.29	422.56	510.5
600	231.04	325.62	484.36	549.08
700	252.1	307.51	534.74	625.46
800	273.3	369.85	588.06	697.17
900	291.68	416.9	637.49	750.64
1000	310.38	443.71	682.17	854.76
1700	428.14	623.94	984.24	1241.12
2000	470.33	691.8	1095.08	1384.92

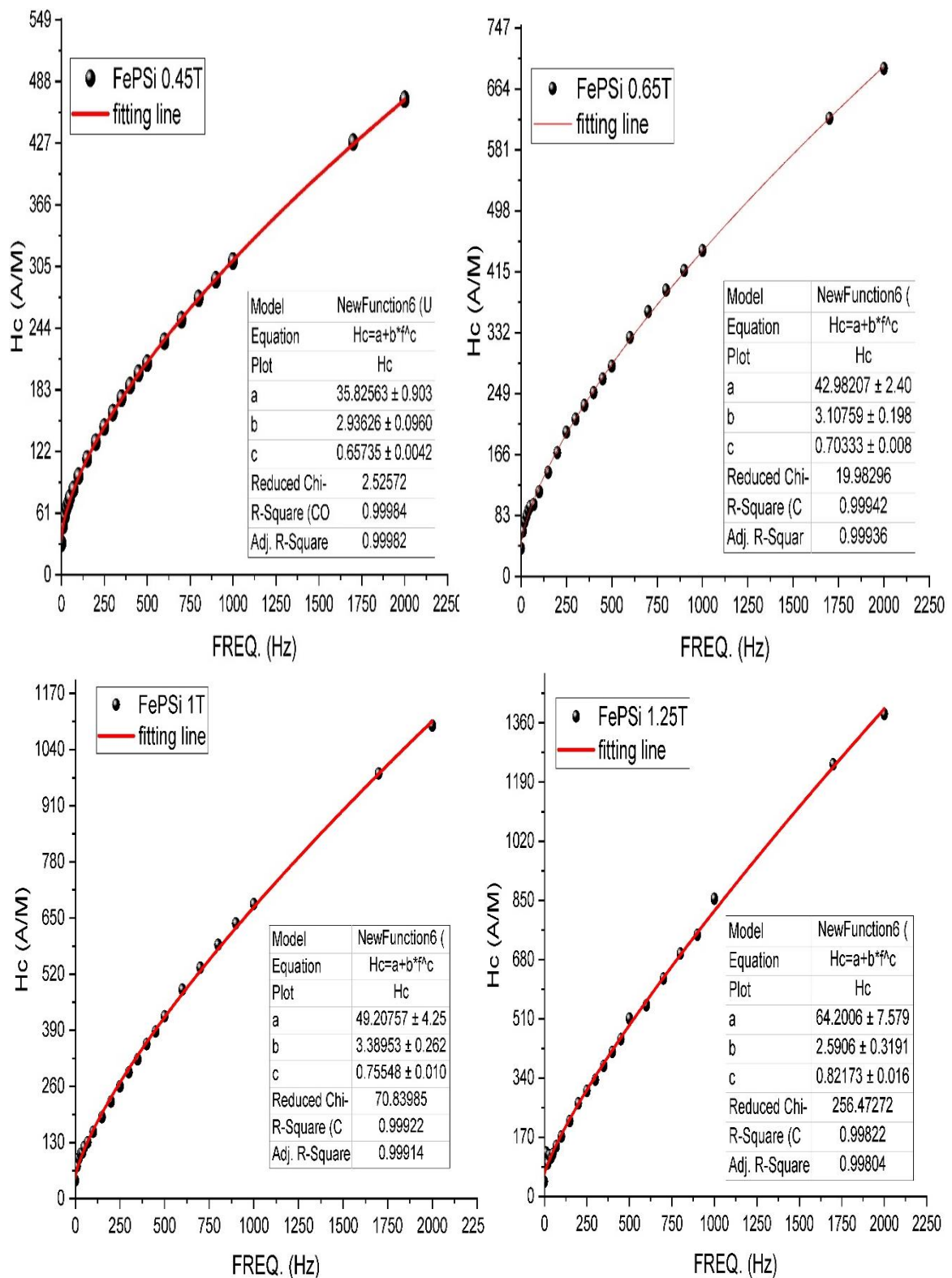


Figure 5.1(i): Fitting on the frequency dependent coercivity on different magnetic field on Fe-P-Si according eq (25) (a)B=0.65, (b)B= 0.45T, (c)B=1T, (d)B=1.25T

Table 5.1(b) Fitting Parameters for Equation (25):

C	a	a	Δa	b	Δb	c	Δc
0.45T	35.82	35.82	0.90	2.93	0.09	0.65	0.004
0.65T	42.98	42.98	2.4	3.10	0.19	0.70	0.01
1T	49.20	49.20	4.2	3.38	0.26	0.75	0.01
1.25T	64.2	64.2	7.57	2.59	0.31	0.82	.0.01

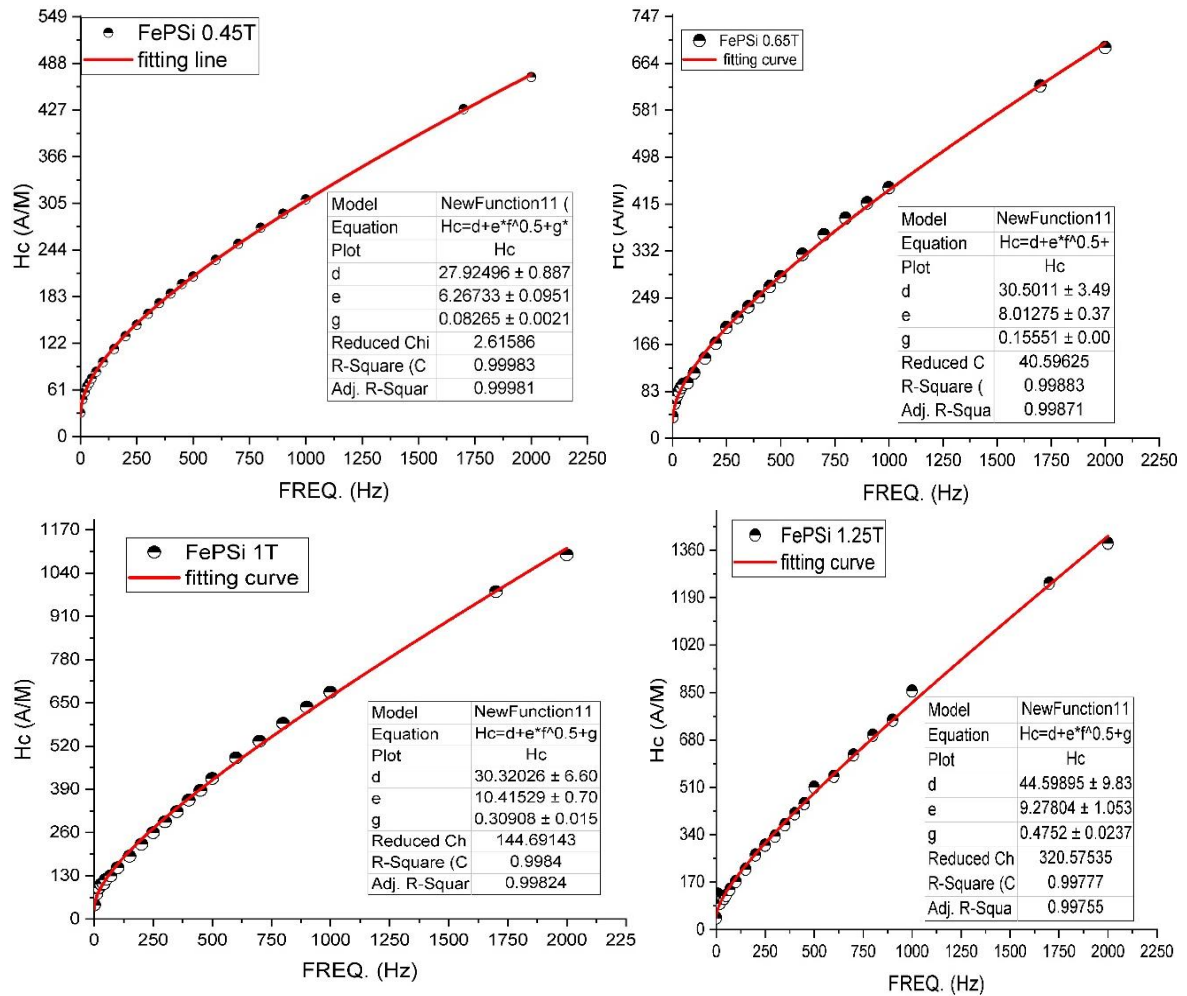


Figure 5.1 (ii): Fitting on the frequency dependent coercivity on different magnetic field on Fe-P-Si according to equation (26)

Table 5.1(): Data for Fitting Parameter in H_cVs Frequency Curve for Equation (26):

Magnetic field (B)	d	Δd	e	Δe	g	Δg
0.45T	27.92	0.68	6.3	0.095	0.08	.002
1T	30.32	0.70	10.4	0.07	0.3	.0015
0.65T	44.5	3.4	8.01	0.37	0.15	0.00
1.25T	30.5	9.8	9.27	1.05	0.47	0.02

Frequency dependence of coercivity (f) was analyzed by fitting the data by two general equations 24 and 25 as already described in above part. Frequency dependence of the coercivity in amorphous materials, has been analyzed by the Eq. 25 derived for triangular wave form of the field with and we get to know that the high value of c ($c = 0.8$) means also that normal and anomalous eddy currents are existing.

5.2 DC Hysteresis:

Bertotti's work proved that iron losses can be decomposed in different components: hysteretic losses from DC measurements, eddy current losses due to eddy current circulation in the sheet and excess losses. Excess losses are generated by wall motion dynamic in the structure of the sheet under magnetic field circulation. To complete the study on iron losses, DC hysteresis has to be measured for each level of magnetic flux density. The DC hysteresis corresponds to a complete cycle of magnetization without any effect of the frequency. **[Figure 5.2]** shows the DC hysteresis at different magnetic field for Fe-P-Si. Few parasites on the H signal are observed on the cycle. They are due to switching H for a same B point and linked to process of DC loop magnetization. They do not really influence the measurement data. The area of the loop is equal to the magnetic energy in Joule consumed in the sheet per m^3 per hysteresis cycle. In order to have DC or hysteretic losses in Watt per kg at each frequency, the energy per m^3 is multiplied by the corresponding frequency and divided by the density.

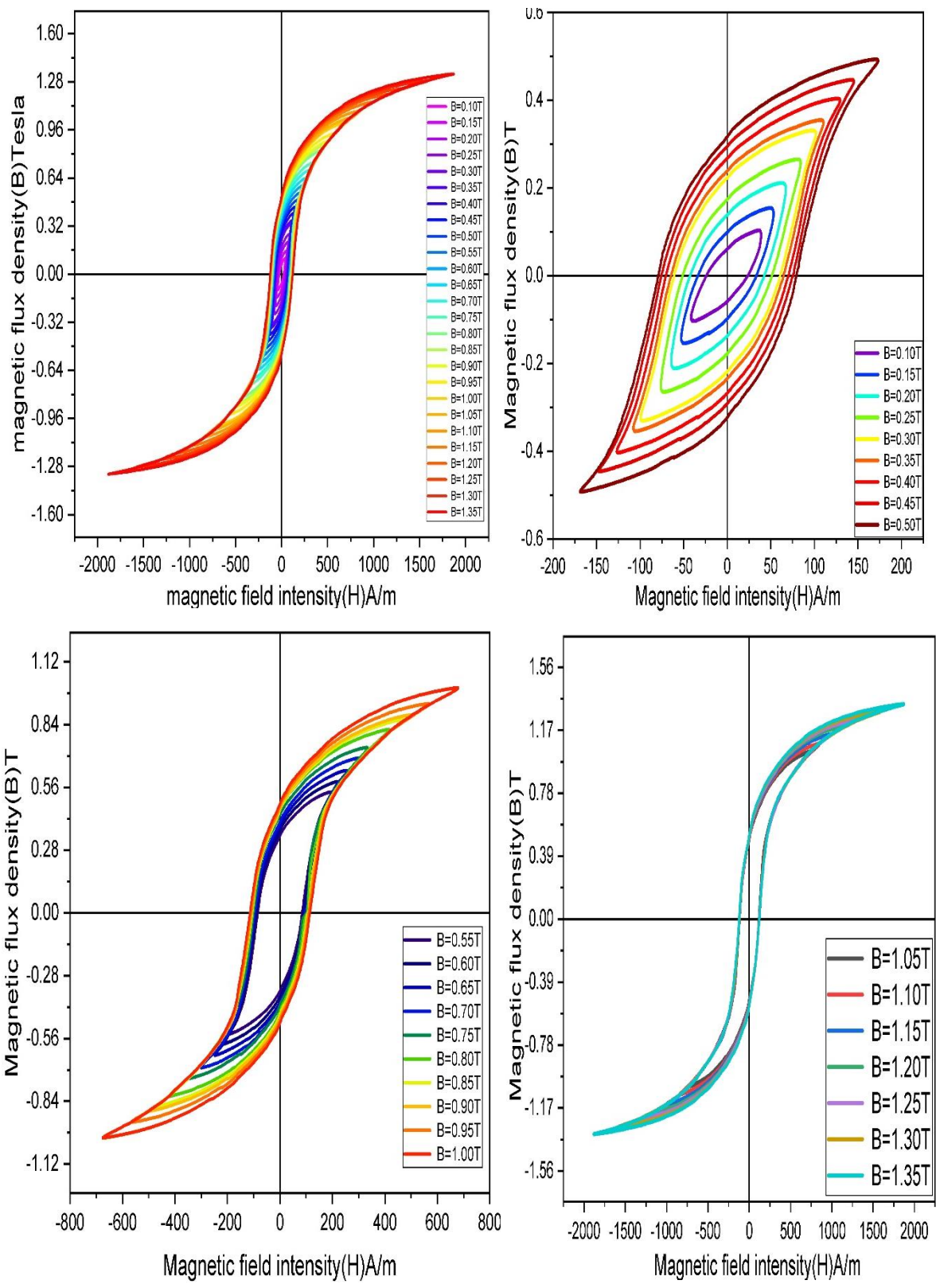


Figure 5.2: BH loop measurement at DC

5.3. Frequency Depended Hysteresis:

Magnetic hysteresis was measured on hysteresis graph described in method. Ring shaped samples were exhibited with primary and secondary windings. Samples with their geometry dimensions and parameters used for hysteresis measurements. All magnetic measurements were performed under triangular magnetizing current in order to obtain constant dH/dt . The samples were demagnetized before each measurement. The hysteresis loss subdivision method proved to be a strong tool to help in the analysis of different energy dissipation mechanisms along the quasi-static hysteresis loop measured on electrical steels. were measured under triangular waveform excitation at high frequency to 10kHz to 3500kHz. The results show a different behavior between the low inductions hysteresis loss (WLI) and the high induction hysteresis loss (WHI) which proves the existence of different energy dissipation mechanisms affecting these loss components.

We are measuring the Hysteresis curve of our sample Fe-P-Si at different frequency in different magnetic fields.

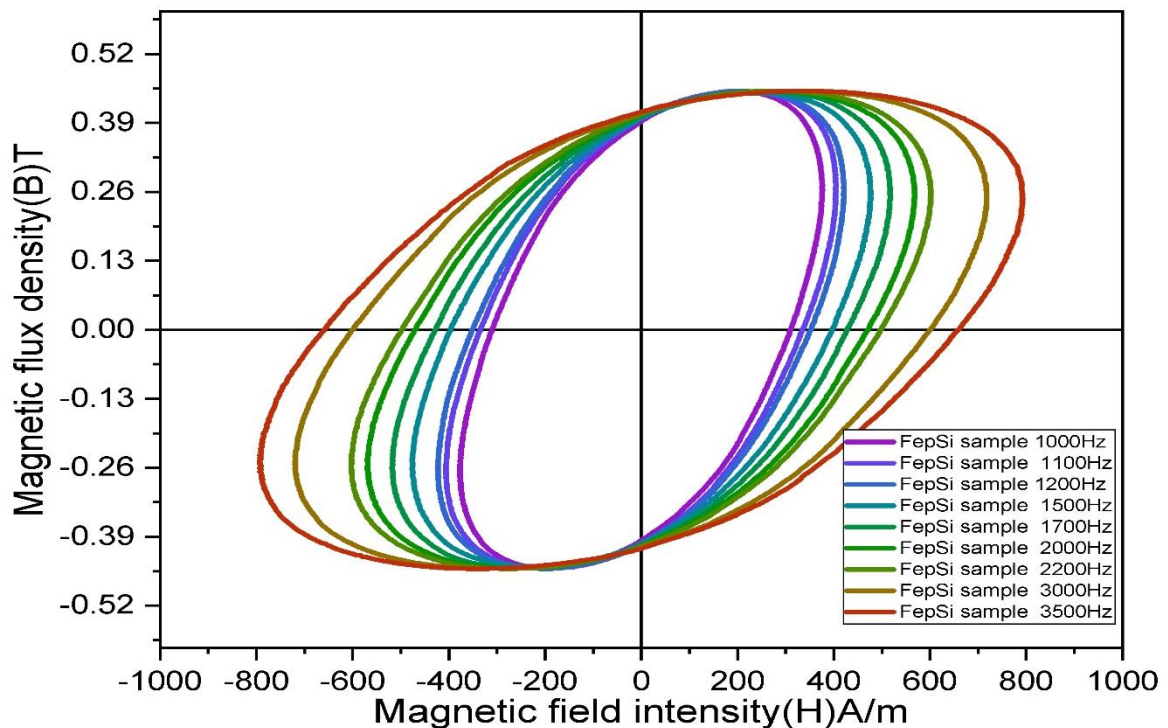


Figure 5.3 (a): Magnetic hysteresis measurements at 0.45T, Swelling-up of hysteresis with frequency

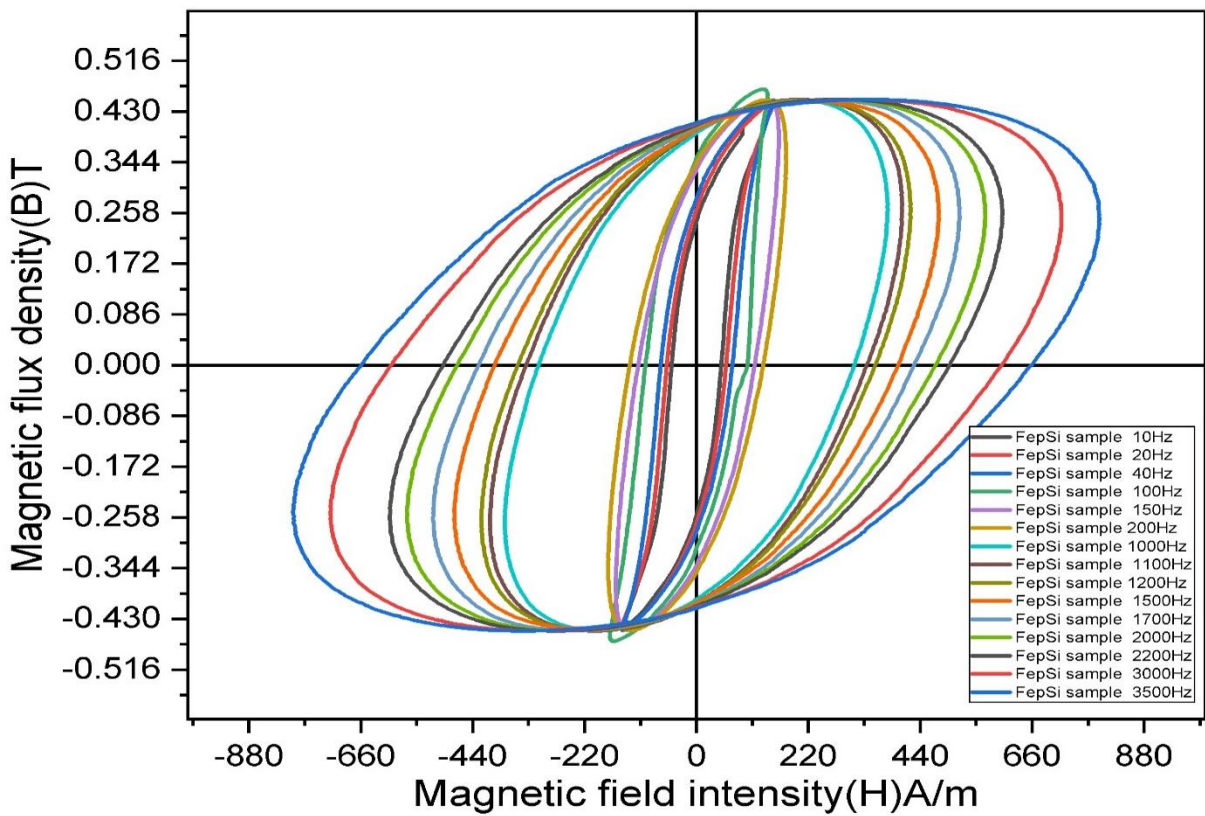
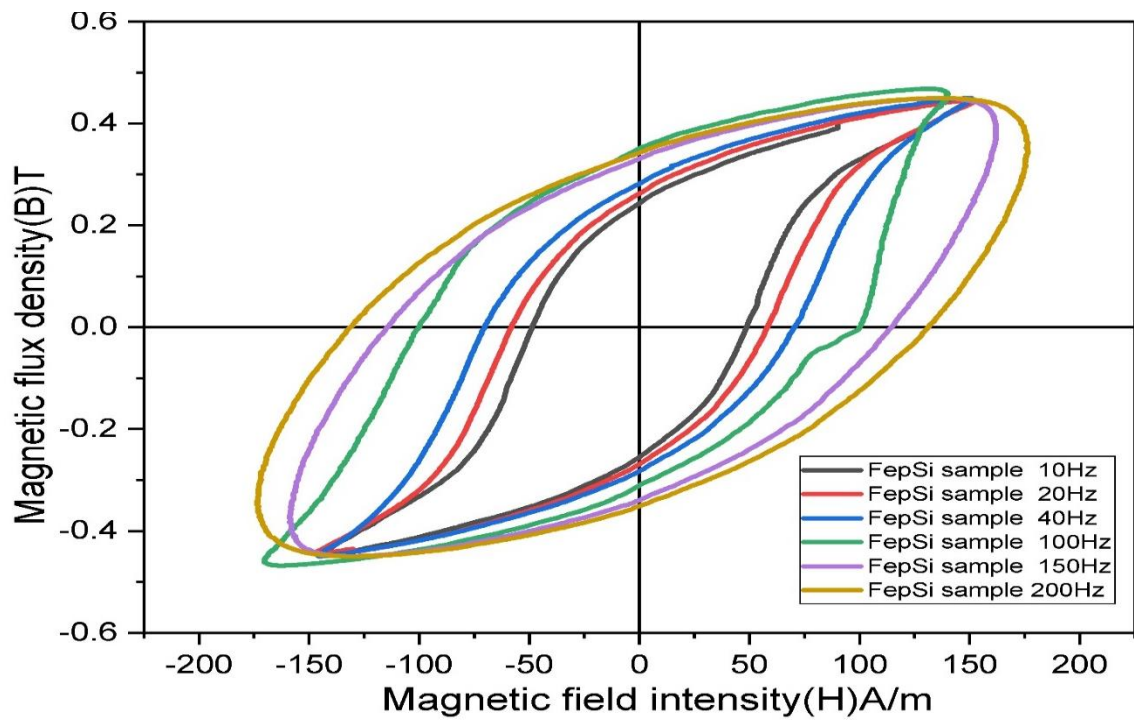


Figure 5.3 (a): Magnetic hysteresis measurements at 0.45T, Swelling-up of hysteresis with frequency

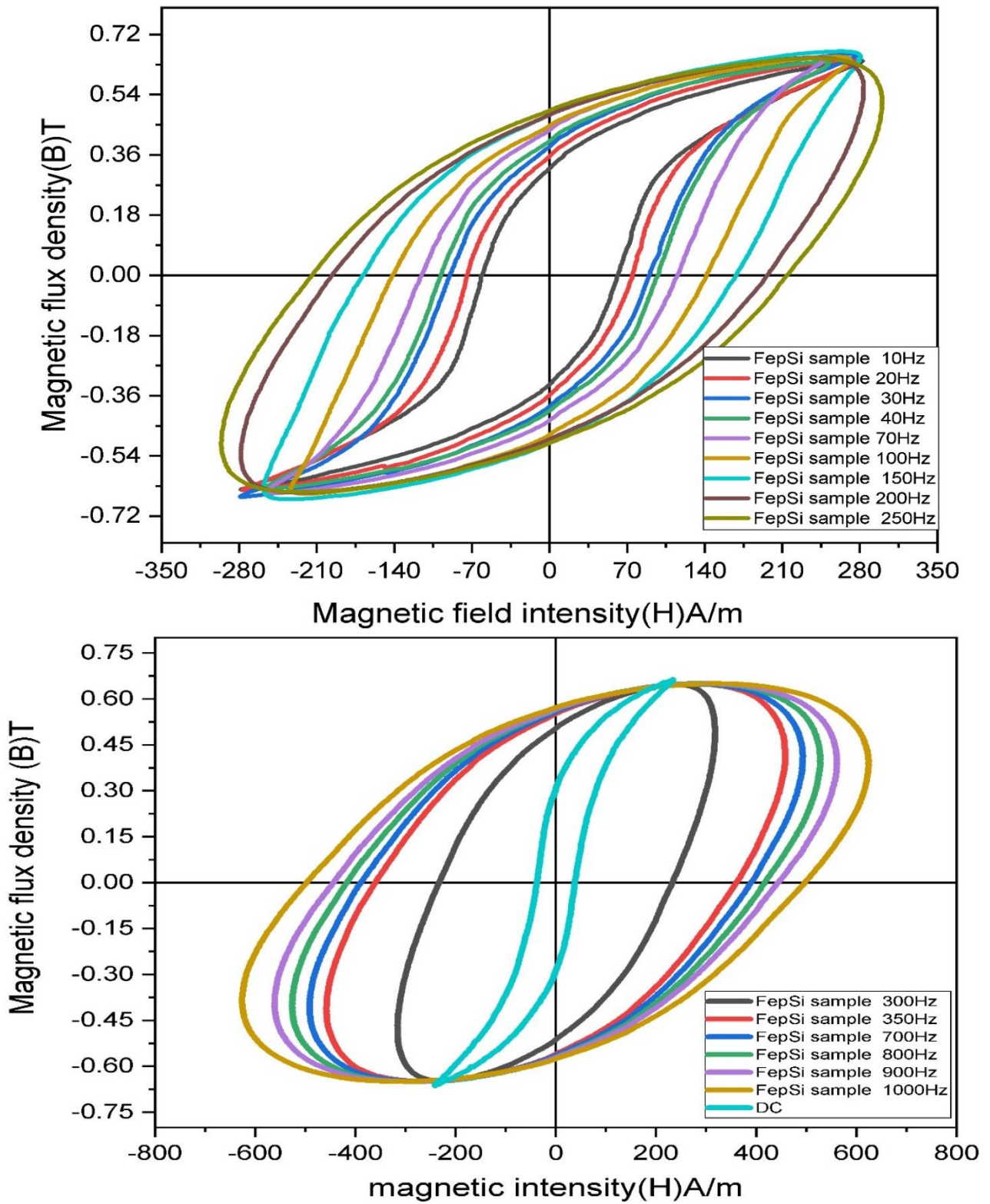


Figure 5.3 (b): Magnetic hysteresis measurements at 0.65T, Swelling-up of hysteresis with frequency

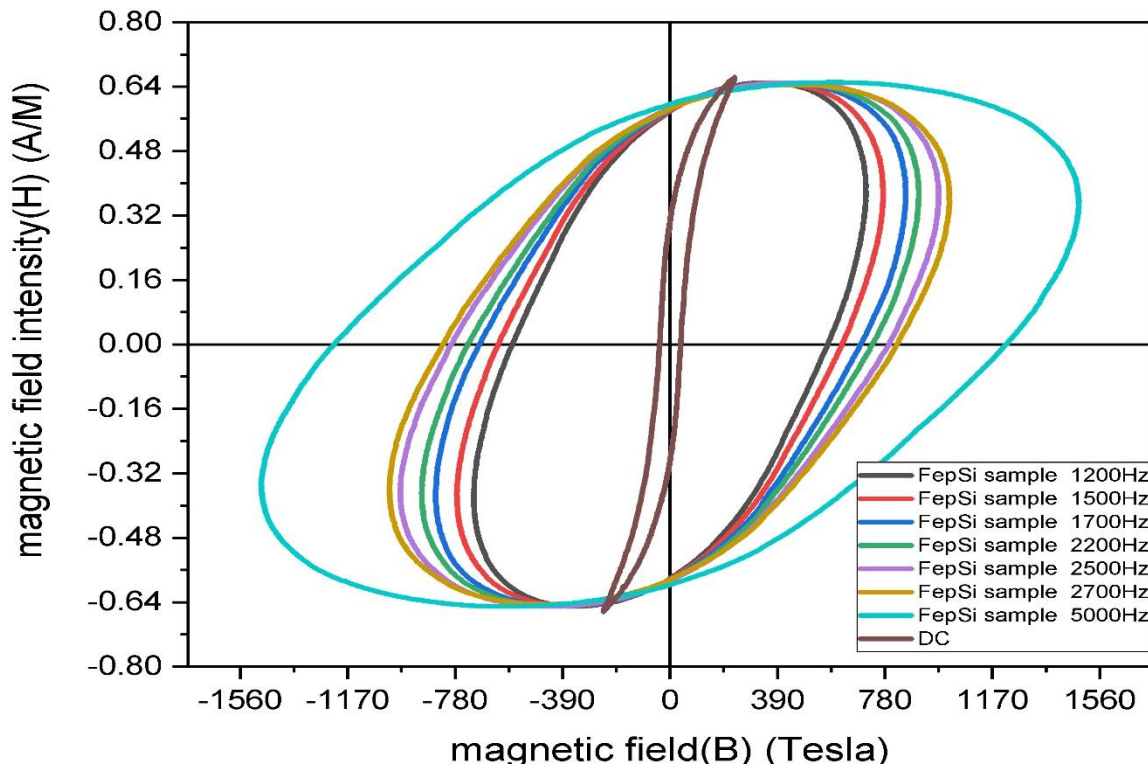


Figure 5.3 (b): Magnetic hysteresis measurements at 0.65T, Swelling-up of hysteresis with frequency

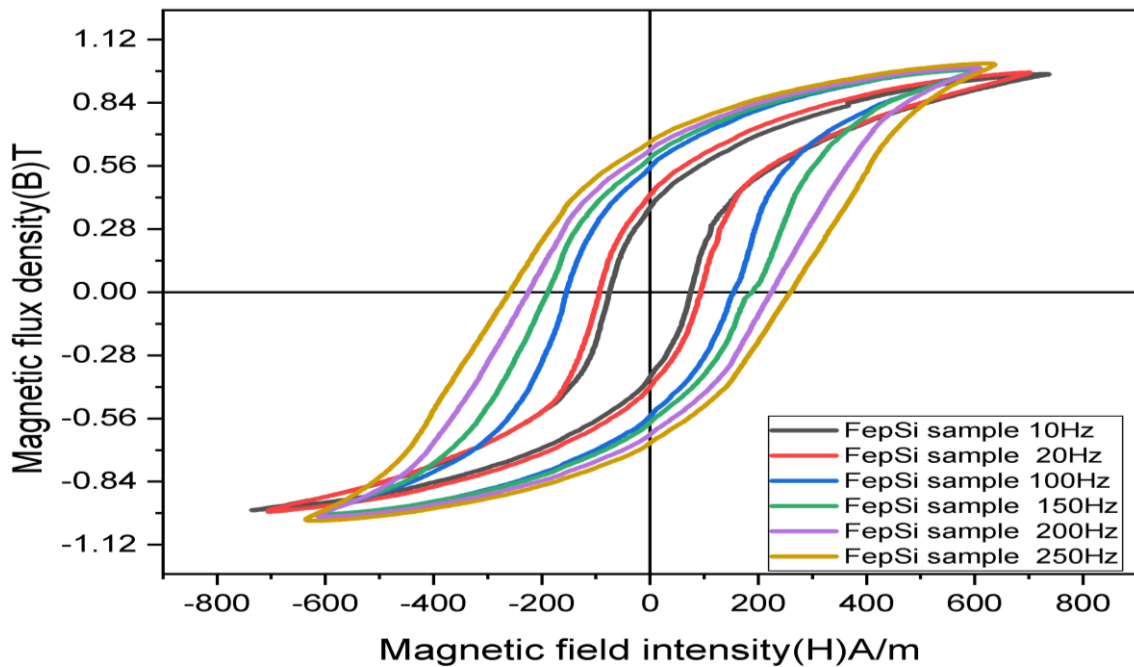


Figure 5.3 (c): Magnetic hysteresis measurements at 1T, Swelling-up of hysteresis with frequency

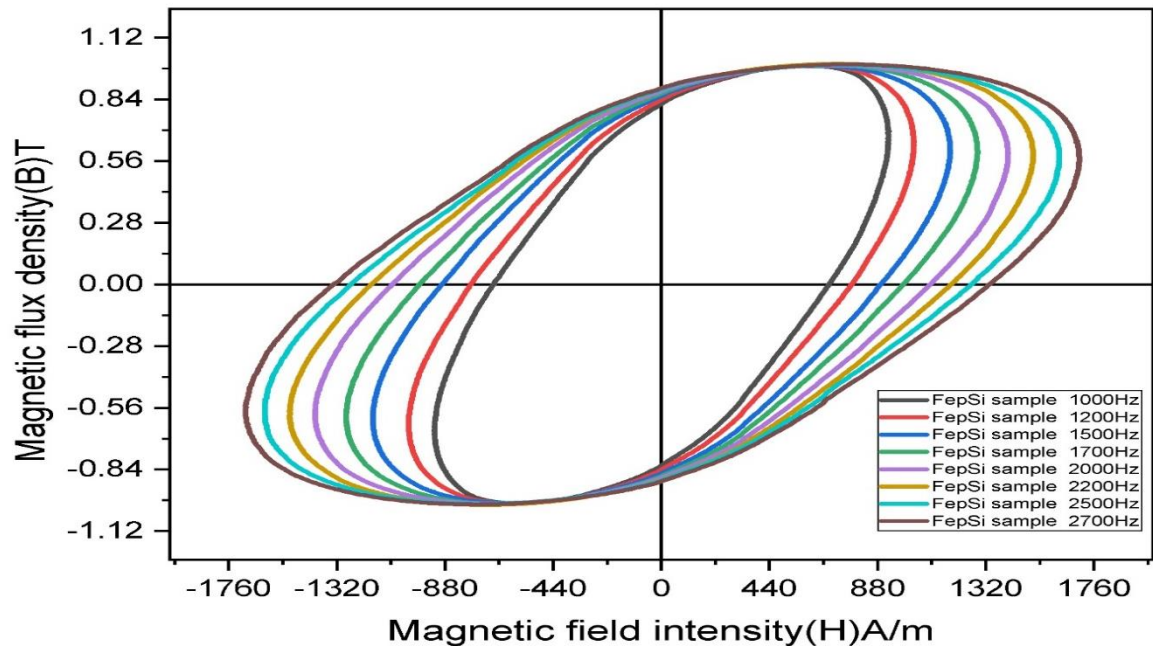


Figure 5.3 (c): Magnetic hysteresis measurements at 1T, Swelling-up of hysteresis with frequency

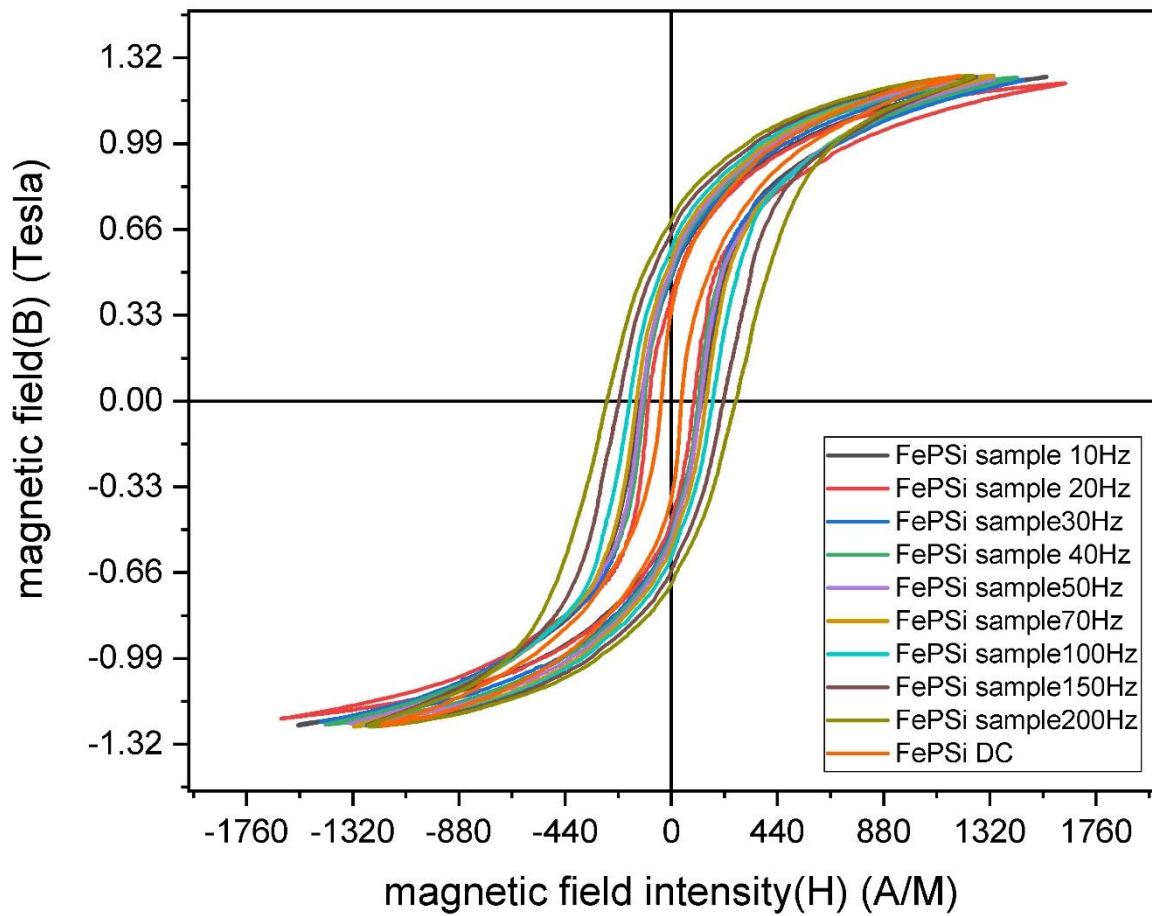


Figure 5.3 (d): Magnetic hysteresis measurements at 1.25T, Swelling-up of hysteresis with frequency

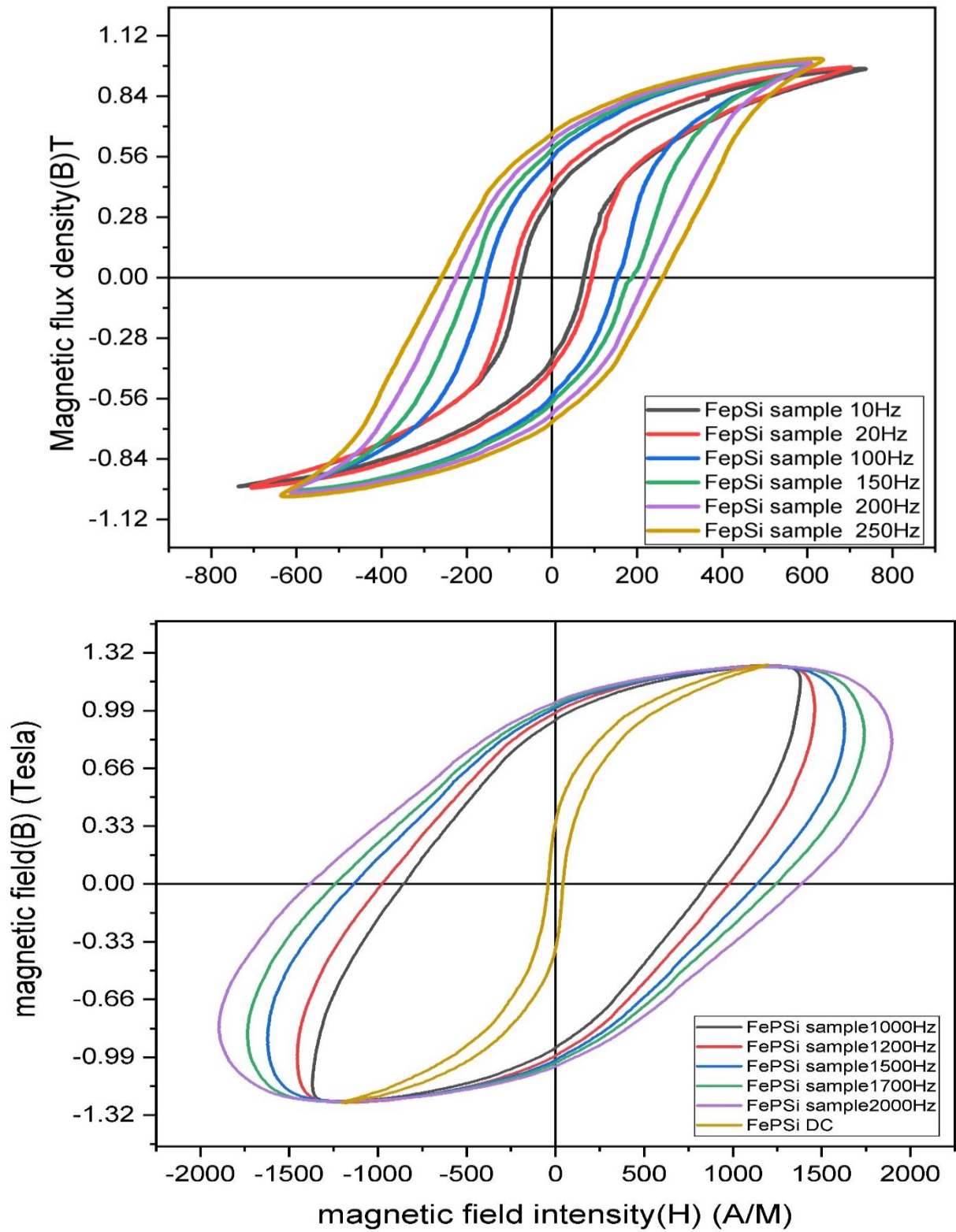


Figure 5.3 (d): Magnetic hysteresis measurements at 1.25T, Swelling-up of hysteresis with frequency

In the following figure hysteresis cycles are plotted from 3000kHz to 10 Hz. The frequency effect clearly manifests itself by an enlargement of the hysteresis loop area. First, to characterize the frequency influence, sinusoidal waveforms of B are preferable to determine the general behavior easily. Thus, we measure different magnetic quantities by varying the frequency from 10Hz to 3000KHz at several level of magnetic flux density B . These levels (0.45T, 0.65T, and 1.25T) are chosen in order to reproduce material magnetization under different conditions. we have decided to limit the B magnitude at 1.25T to ensure all the measurements for each frequency. Then, DC hysteresis loops are measured for every B level. Indeed, these measurements are dependent of the frequency and correspond to the hysteretic behavior of losses in magnetic materials.

5.4. Frequency Dependence Relative Permittivity

Eddy current model for $\mu_r = \frac{k}{(H_c f)^n}$

Generally, it can be assumed that the permeability scales reciprocal with the coercivity [Turtelli et al., 2006.]. Therefore, an increasing coercivity due to an increase of the frequency may cause a reciprocal decreasing permeability. This leads to an improved eddy current model by assuming $\mu_r(f)$ as a function of $H_c(f)$ which can be described by the simple formula.

$$\mu_r = \frac{k}{(H_c f)^n} \quad (29)$$

Where k is a choose able fit parameter.

Table:5.2. Data Table for Relative Permeability

frequency Hz	Hv A/M	Bv T	Jv T	Br T	Hc A/M	LOSS W/Kg	H(μ max)	μ max FePSi
0	1001.9	1.191	1.19	0	0	0	0	3454
10	1000.9	1.08	1.079	0	0	0	0	2737
40	1001.9	1.136	1.135	0	0	0	0	2610
50	1000.9	1.146	1.144	0	0	0	0	2629
60	1004	1.157	1.155	0	0	0	0	2465
70	1000.9	1.163	1.161	0	0	0	0	2508
80	1033.1	1.178	1.177	0	0	0	0	2454
90	1001.4	1.17	1.169	0	0	0	0	2429
100	1001.9	1.171	1.17	0	0	0	0	2441
200	1003.4	1.177	1.175	0	0	0	0	2055
300	1004	1.179	1.178	0	0	0	0	1767
400	1005	1.18	1.179	0	0	0	0	1552
500	1005	1.174	1.172	0	0	0	0	1389
600	1000.4	1.157	1.156	0	0	0	0	1235
700	1002.4	1.151	1.15	0	0	0	0	1140
800	1000.4	1.124	1.123	0	0	0	0	1063
900	999.9	1.094	1.093	0	0	0	0	999
1000	999.9	1.052	1.051	0	0	0	0	934
1100	999.9	1.014	1.013	0	0	0	0	890
1200	1000.4	0.98	0.979	0	0	0	0	851
1300	1001.4	0.942	0.941	0	0	0	0	812
1400	1018.8	0.926	0.924	0	0	0	0	782
1500	999.9	0.874	0.873	0	0	0	0	748
1600	1000.4	0.853	0.852	0	0	0	0	724
1700	1000.4	0.822	0.821	0	0	0	0	696
1800	1001.9	0.799	0.798	0	0	0	0	672
1900	1000.4	0.775	0.774	0	0	0	0	650
2000	1000.4	0.759	0.757	0	0	0	0	634
2500	1000.9	0.674	0.673	0	0	0	0	557
3000	1000.4	0.615	0.614	0	0	0	0	504
3500	1001.9	0.563	0.561	0	0	0	0	459
4000	1001.9	0.529	0.527	0	0	0	0	428
4500	1006	0.501	0.499	0	0	0	0	401
5000	1000.4	0.47	0.469	0	0	0	0	377

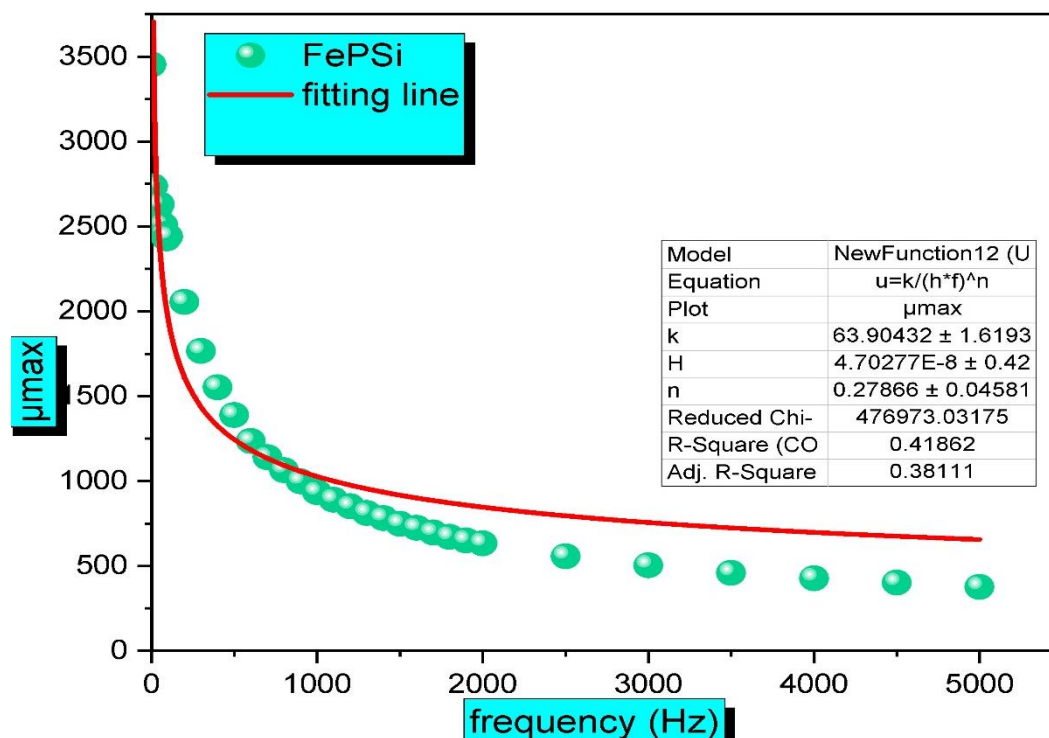


Figure.5.4 frequency vs relative permeability curve fitting

5.5. Frequency dependent Total losses:

Steinmetz's Two-Term Model:

The idea was to develop a simple formula which depends only on the flux density and frequency. A formula composed of hysteresis and eddy current components was deduced and is given by

$$P = K_h B_p^n f + K_e B_p^2 f^2 \quad (30)$$

where P is the average loss per unit mass at frequency f and peak flux density Bp, Steinmetz's constant n=1.6, kh and ke are hysteresis and eddy current loss constant coefficients respectively

Table-5.3: Data Frequency and Total Core Losses

Frequency Hz	loss W/Kg 0.45T	loss W/Kg 0.65T	loss W/Kg 1T	loss W/Kg 1.25T
0	0	0	0	0
10	0.089	0.166	0.338	0.611
20	0.211	0.414	0.838	1.13
30	0.35	0.689	1.278	2.022
40	0.51	1.007	1.867	2.843
50	0.706	1.279	2.518	3.737
70	1.117	1.902	3.942	5.995
100	1.965	3.256	6.67	9.972
150	3.324	6.016	12.309	18.716
200	5.083	9.812	20.155	30.279
250	7.102	13.885	29.787	43.761
300	9.359	18.348	40.041	59.247
350	11.932	23.336	53.042	77.538
400	14.584	28.535	67.842	99.054
450	17.634	34.844	83.495	121.284
500	20.647	41.114	94.387	151.544
600	27.486	56.269	130.585	194.413
700	35.073	72.961	167.49	258.374
800	43.463	90.215	211.08	331.287
900	52.294	109.519	255.077	416.341
1000	61.628	129.599	302.869	487.352
1200	84.141	173.921	411.529	666.683
1500	117.835	249.632	595.526	957.609
1700	146.369	307.37	744.64	1181.541
2000	189.144	400.259	970.05	1539.007

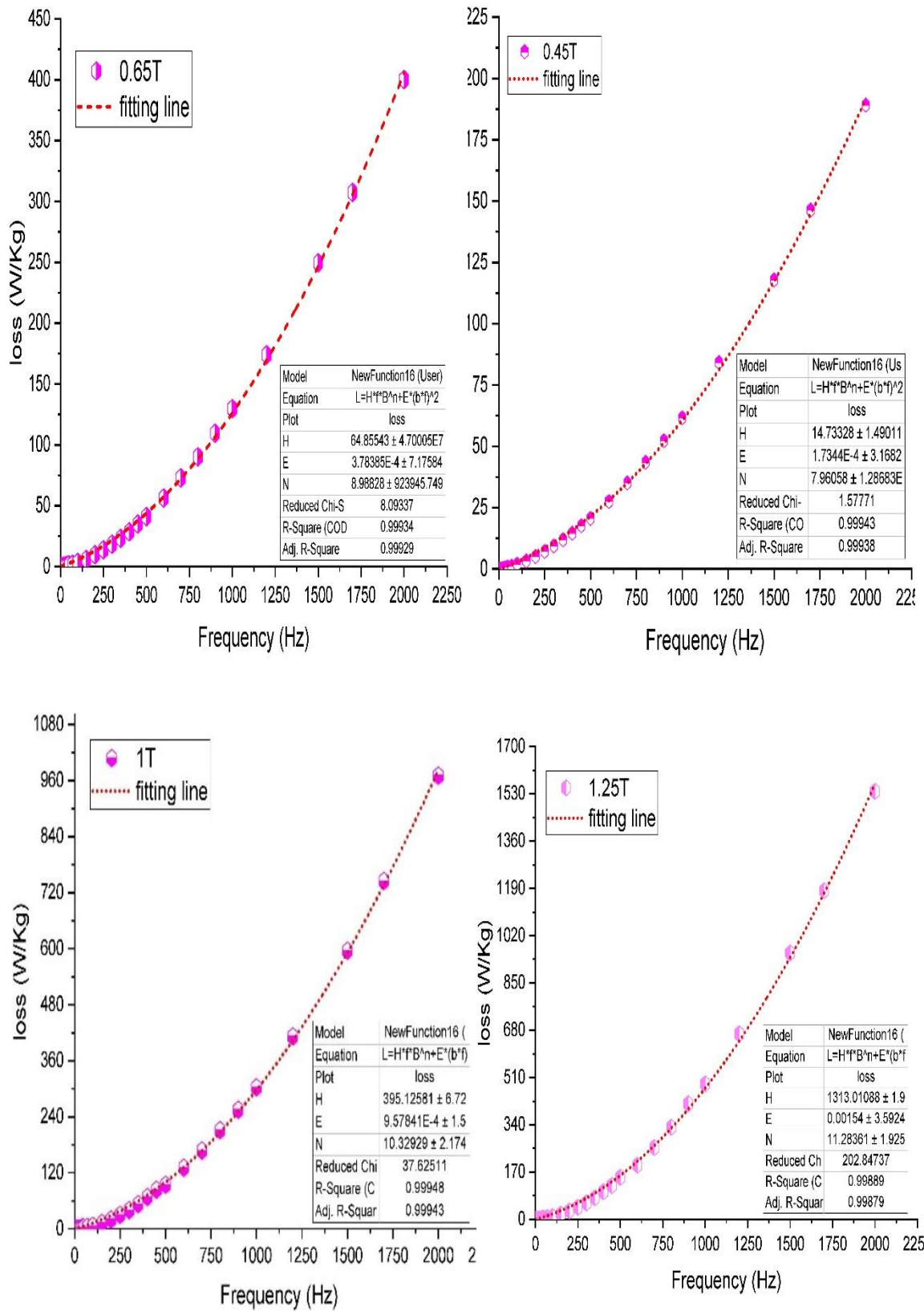


Figure 5.5(a): Fitting data on basis of equation (31), frequency vs core loss

Classical Model with Physical Basis:

Under sinusoidal flux densities, the classical eddy current loss, P_{cl} , takes a form of

$$P_{cl} = \frac{\sigma \pi^2 d^2}{6\rho} B_p^2 f^2 = K_{cl} B^2 f^2 \tag{31}$$

where, σ and d are material conductivity, density and thickness respectively.

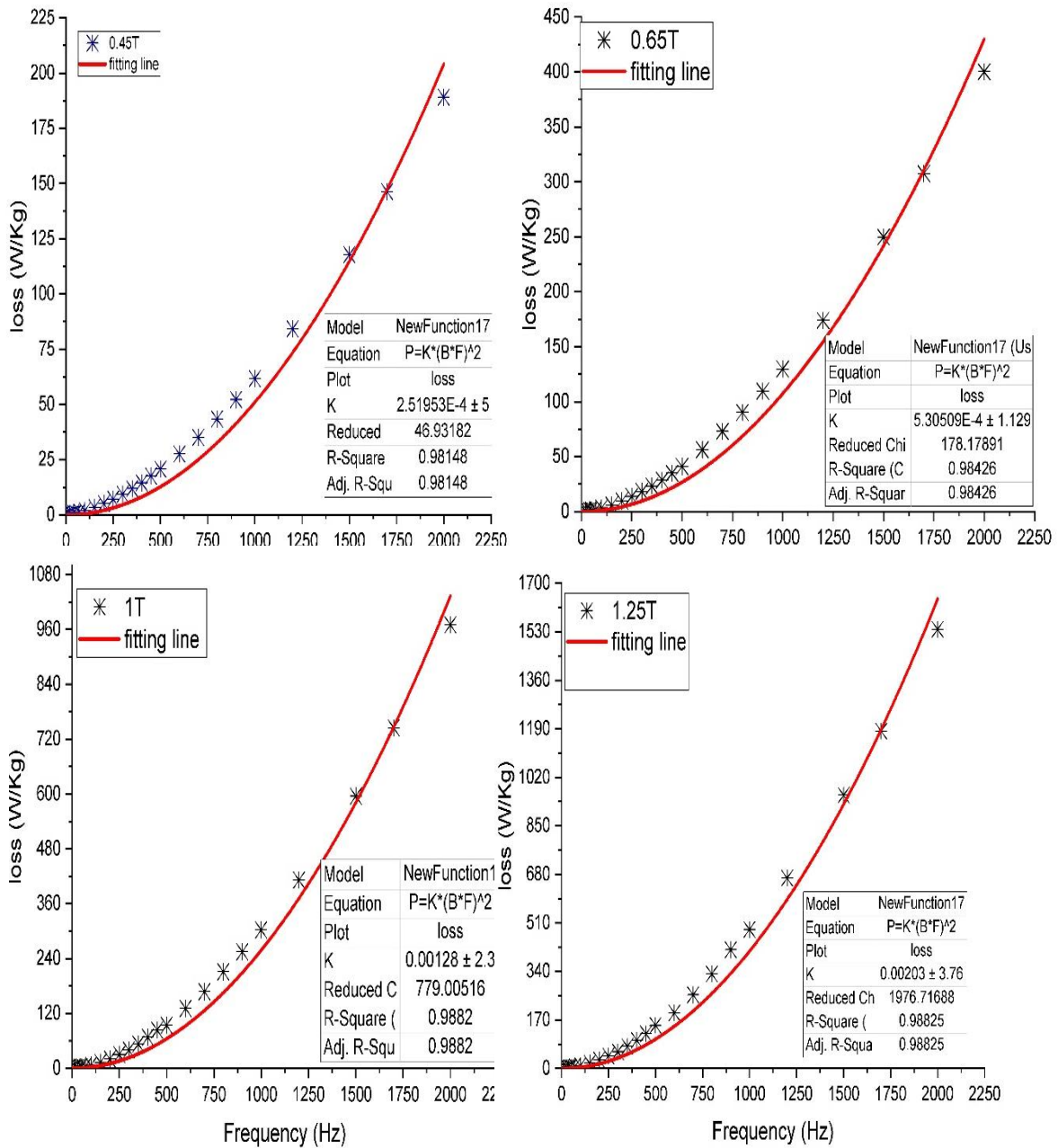


Figure 5.5(b): Fitting data on basis of equation (31), frequency vs core loss

Steinmetz and Classical Model Comparison:

A comparison between equations (30) and (31) is now examined. In this case, the Steinmetz's formula (30) is compared with (31) for $n = 1.6$ in both equations. Steinmetz's test results are limited to high frequencies is made to test validity at high frequencies.

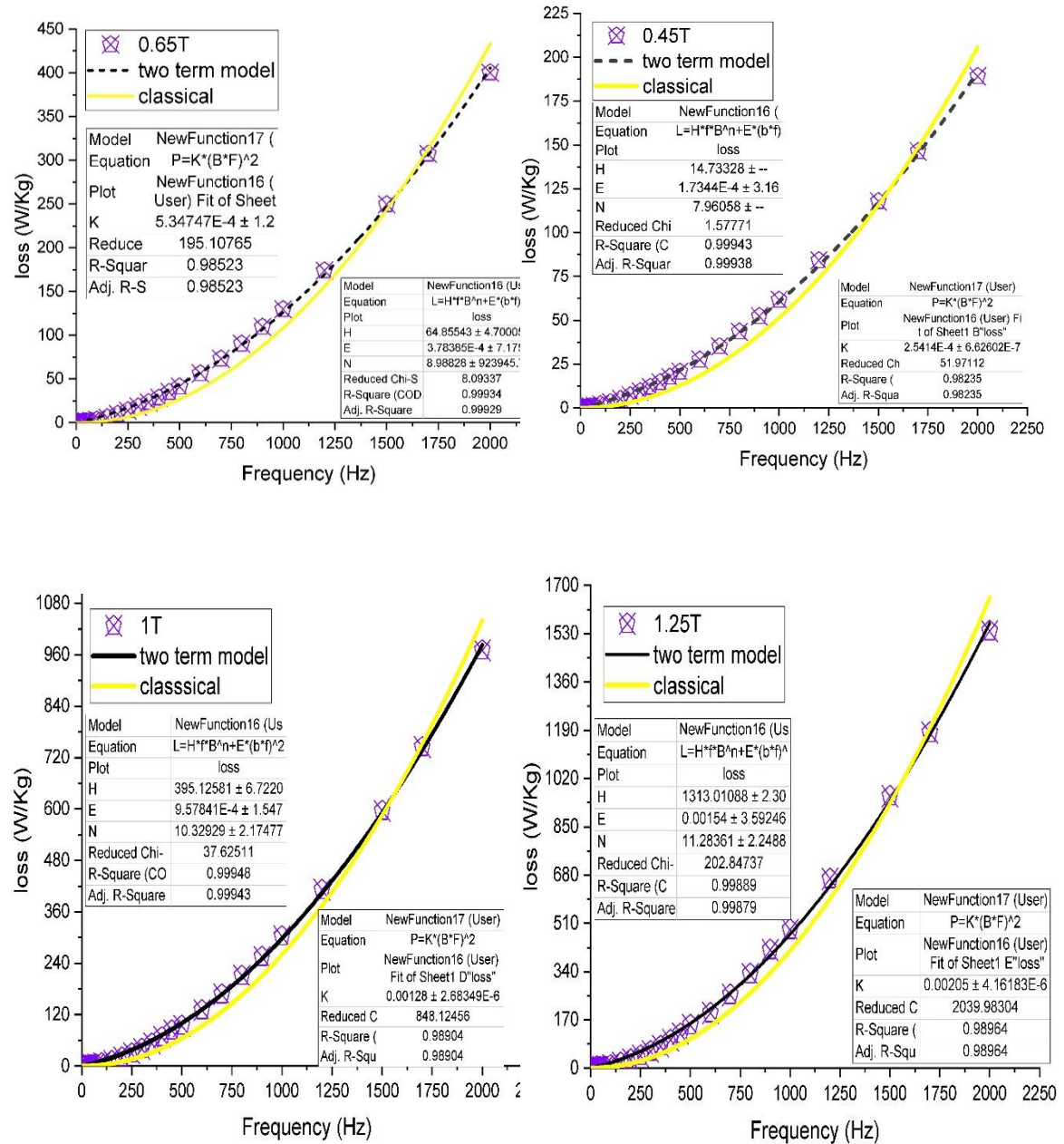


Figure 5.5(c): Steinmetz and Classical Model Comparison:

Improve core loss models:

An improved formula with a physical basis for the variation of loss coefficients with flux density and/or frequency developed by Lotten in using the test bench results is presented and tested here. Furthermore, an alternative averaging method of excess loss coefficient is presented as a modification in order to reduce the computation time. The new formula is an extension of Bertotti's formula. The improved formula has good accuracy at high flux densities and frequencies, and takes a form of

$$P = P_h(f, B) + k_e(f)B_p^2 f^2 + K_{ex}(f, B)f^{1.5}B^{1.5} \quad (32)$$

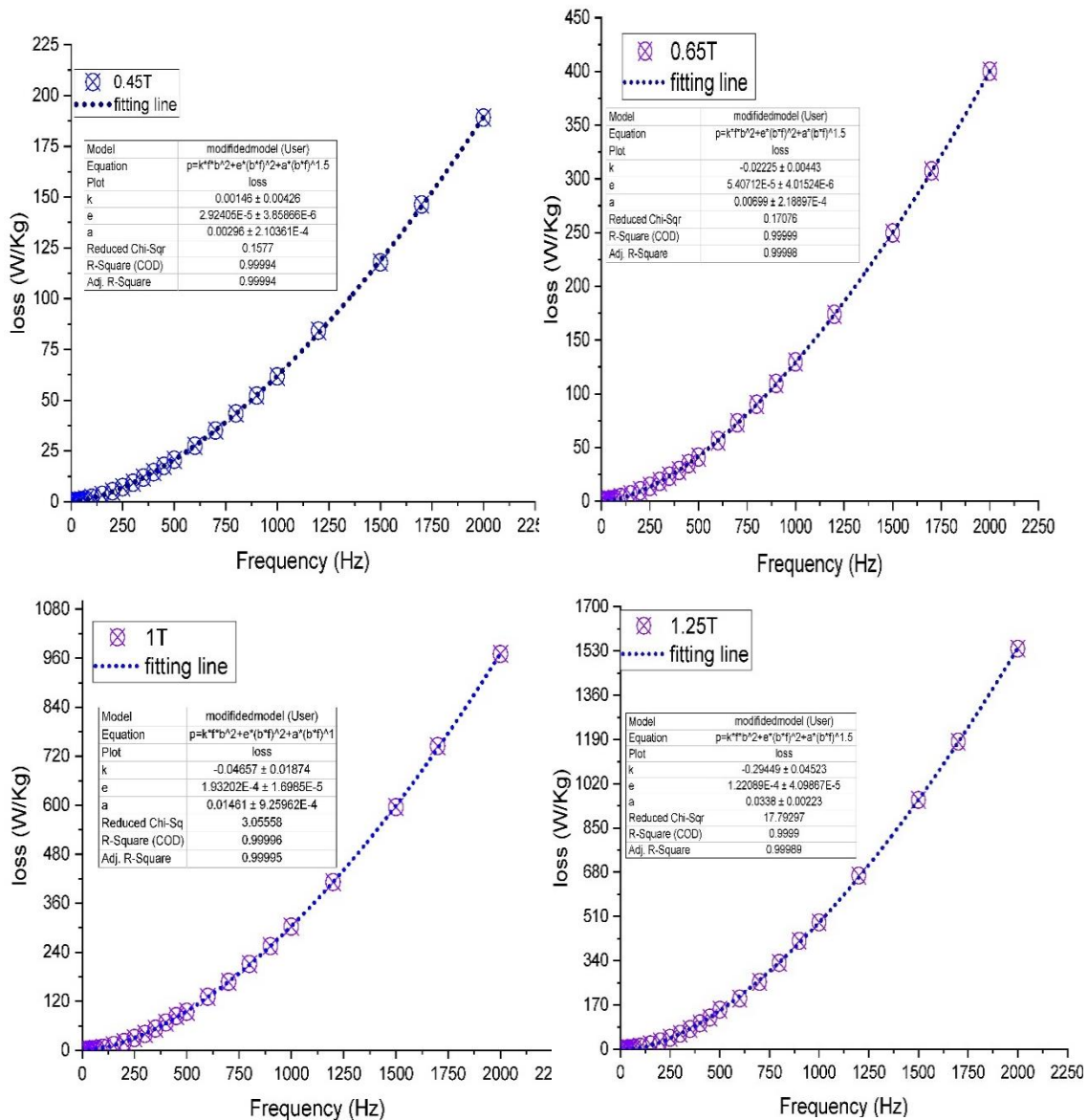


Figure 5.5(d): Fitting data on basis of equation (32), Improve core loss models

Steinmetz, Classical Model and improve core loss model Comparison:

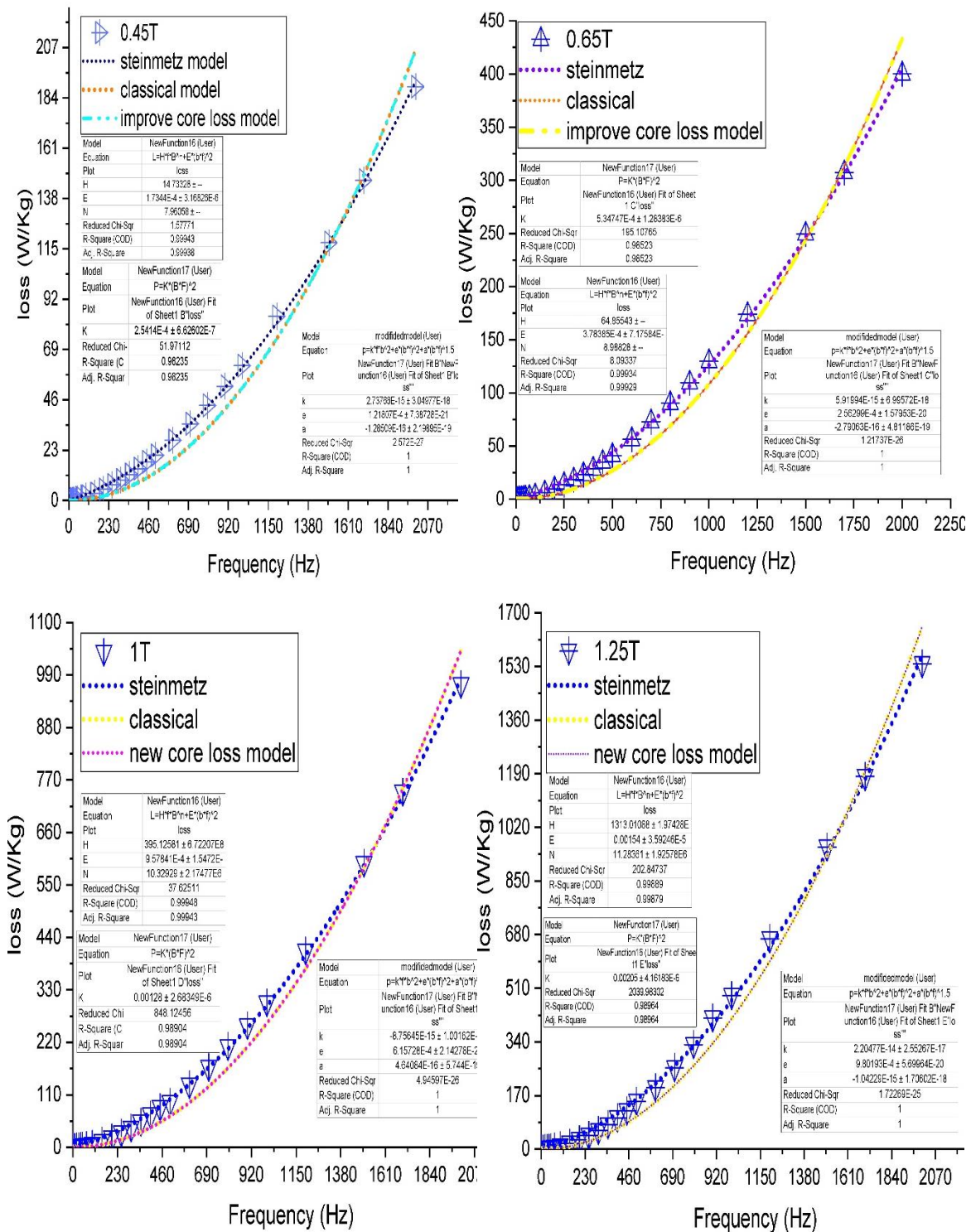


Figure 5.5(d): Steinmetz, Classical Model and improve core loss model Comparison

CHAPTER 6: DISCUSSION

6. Discussion

6.1. Discussion Frequency Dependent Coercivity:

Frequency dependence of coercivity $H_C(f)$ was analyzed by fitting the data by two general equations 22 and 23 as already described in previous part

In Eq. (22) it is assumed that $H_C(f)$ scales with some unknown power of f and in Eq. (23) $H_C(f)$ expressed into different powers of f . The fit parameters a and d corresponds to coercivity at zero frequency i.e. $H_C(f=0)$. b , c , e and g are fitting parameters. The coefficient b and the power factor c in Eq. (22) deliver an average of normal and anomalous eddy currents. The coefficients e and g describe the normal eddy and anomalous eddy currents respectively. The result of the fitting is shown in [Figure 5.1]: and the fitting parameters are given in [Table 5.1(b)]: Frequency dependence of the coercivity in amorphous materials, has been analyzed by the Eq. 23 derived for triangular wave form of the field with

With H_0 is the field amplitude, $H_C(0)$ is the coercivity at zero frequency, the coefficient depending on intrinsic parameters of materials, and n can vary between 1 and 3 depending on the geometry and on the microstructure of the material as well as on the considered frequency range [Zhukov et al., 2009]. Eq. (23) and (22) are set equivalent; from this the coefficient b can be expressed as $B = b/(H_0)^{1/n}$ which correlates then the dynamic coercivity field. The value of power factor c_s obtained by fitting which is in accordance with the range mentioned [Zhukov et al., 2009]. The high value of i.e. ($c = 0.8$) means also that normal and anomalous eddy currents are existing.

6.2 Discussion DC Hysteretic Behavior:

In DC hysteresis loop, when we increase magnetic field then the magnetic field intensity creates magnetic flux density. So, we can describe the B-H loop at different magnetic field at DC condition. Here we use soft iron-based material and it will have its own set of magnetic hysteresis curves. In the above graphs in DC condition, we see that the magnetic flux density changes unto 0.5 T when magnetic field changes from 0.10 T to 0.50 T. When we increase the magnetic field from 0.55 T to 1.00 T then the magnetic flux density changes unto approximately 1 T. If we further increase the magnetic field then the magnetic flux density increases. We increase magnetic field from 1.05 T to 1.35 T then magnetic flux

density changes up to approximately 1.2 T. And further if we increase the magnetic field, the magnetic flux density remains same. So, we say that it gets saturation. The cause of this case is that there is a limit to the amount of flux density that can be generated by the core as all the magnetic domains in the iron becomes perfectly aligned. The point on the graph where the magnetic flux density reaches is the limit, is called Magnetic Saturation also known as saturation of the core.

6.3 Discussion on AC Hysteretic Behavior:

The area of hysteresis loop describes the total loss of the materials at different frequencies. Here, we plot the graph of magnetic flux density vs magnetic field intensity at several levels of magnetic field B (0.45 T, 0.65 T, 1 T, 1.25 T). In [figure 5.3(a)]: we plot two graphs for different frequency range at magnetic field 0.45 T. In the first graph we vary frequency from 10 Hz to 200 Hz and the peaks are at approximately 0.48 T in both positive and negative regions. By increasing the frequency from 1000 Hz to 3500 Hz then the loops are bulged and the area under the curve increases i.e., total loss increases. But the peaks are at 0.48 T as the magnetic field same.

At $B = 0.65$ T, when the frequency increases from Dc to 200 Hz [In figure 5.3 (b)] then the peaks are approximately at 0.69 T in both positive and negative regions. By increasing the frequency up to 5000 Hz, the loops are bulged but the peaks are at same point in both regions.

At $B = 1$ T, by increasing the frequency from 10 Hz to 250 Hz, the peaks are at 0.98 T [In figure 5.3(c)] in both regions. Further increasing the frequency up to 2700 Hz, the loops are bulged keeping the peaks at same point.

At $B = 1.25$ T, when frequency increases from Dc to 2700 Hz [In figure 5.3 (d)] then the peaks are at 1.25 T in both regions. The area under the curve increases with increase in frequency keeping the peaks at same point.

So, the total losses increase by increasing the frequency keeping the magnetic flux density at same point at fixed magnetic field in ac application. Here we see that the magnetic core can't operate in high frequency of AC application i.e. loss is high at high frequency.

6.4 Discussion on relative permeability

The eddy current model modified on the basis of general assumption that permeability and coercivity is reciprocally related, which implies that with an increasing coercivity due to an increase of the frequency may cause a reciprocal decrease in permeability with assumption

$$\mu_r = \frac{K}{(H_c f)^{n \wedge n}}$$

whereas k and n are fitting parameters was applied on the data of frequency dependence coercivity at room temperature.

The value of fitting parameter k also used to calculate the relative permeability at $f=0$ of all samples by using relation is given The maximum relative permeability obtained for un-deformed samples is unreasonable high, however for deformed samples the value is in an acceptable range .Nevertheless the obtained values of maximum relative permeability follow the general assumption that permeability and coercivity is reciprocally related which can be seen from the general trend that a higher coercivity is accompanied by a lower permeability.

The value of n for Fe and un-deformed Fe-Si/Co alloys is nearly equal to 1, which implies that relative permeability is much dependent on the coercivity, however the value of n obtained for our sample Fe-P-Si s is much less than 0.5, which indicate that that the relative permeability is less corelated to the coercivity. The reason might be the general reduction of eddy currents in these samples.

6.5 Discussions Frequency dependent Total losses

Steinmetz's Two-Term Model

The first core loss formula originated from Steinmetz's work in 1892. He performed several core loss experiments on different magnetic circuits excited with sinusoidal currents of frequencies up to 205Hz. From the experimental results, core loss per cycle is plotted vs. flux density at various frequencies and a mathematical expression is sought through curve fitting - an Engineering approach. The idea was to develop a simple formula which depends only on the flux density and frequency. A formula composed of hysteresis and eddy current components was deduced and is given by

$$P = K_h B_p^n f + K_e B_p^2 f^2 \quad (30)$$

where P is the average loss per unit mass at frequency f and peak flux density B_p, Steinmetz's constant n = 1.6, k_h and k_e are hysteresis and eddy current loss constant coefficients respectively. The coefficients k_h and k_e are obtained from measured core loss data at each frequency and averaged where applicable to get a generic formula applicable for all tested frequencies. 10% maximum deviation from measured results has been reported in. For engineering applications, only two measured core loss data are required to calculate k_h and k_e with n = 1.6 or known, else a minimum of three data points is required

Classical Model with Physical Basis

Work has been done in studying the physical origin of eddy current losses and modeling these losses using a physics-based approach. The eddy current losses are caused by the currents generated by the voltages due to changes in magnetic flux density. Therefore, the eddy current loss component was derived using a set of Maxwell's equations below,

$$\nabla \times H = J \quad (31)$$

$$\nabla \times E = -\frac{\partial B}{\partial t} \quad (32)$$

$$J = \sigma E \quad (33)$$

where H, E, J and B are magnetic field, electric field, current density and flux density vectors. Uniform flux density in the lamination is assumed and the impact of skin effect is neglected. The full derivation is found in. The origin of the work is not known but Graham assumed it to be from Steinmetz's work because of similarities. Under sinusoidal flux densities, the classical eddy current loss, P_{cl}, takes a form of equation (31)

measuring the loss data in a fixed value of n we get the value of K_{cl} very small and around 0.002. however, Equation (31) is invalid when used to predict losses at high frequencies, especially with thick materials. The calculated eddy current loss component becomes much larger than the total measured losses This is because of higher loss coefficient k_{cl} compared to thin materials. It can be concluded that skin effect should be taken into account when using (31), especially with thick materials or high frequencies.

Steinmetz and Classical Model Comparison:

A comparison between equations (30) and (31) is now examined. In this case, the Steinmetz's formula (30) is compared with (31) for $n = 1.6$ in both equations. Steinmetz's test results are limited to an extension to high frequencies is made to test validity at high frequencies.

The loss coefficients are recalculated at each test frequency to give the best possible loss estimates. A negative hysteresis loss coefficient k_h is calculated at 3.2kHz using equation (31). This is because the calculated eddy current component is higher than the total measured losses as shown in [Figure.5.5(c)], and equation (31) compensates the error by subtracting the hysteresis component from the eddy current loss component

The Steinmetz's formula is tested at higher frequencies and does not produce negative loss coefficients like the classical formula. The invalidity observed in (31) at high frequencies can be avoided by considering the skin effect. Low frequency operation avoids the problem altogether. The two formulae under estimate losses at high flux densities.

Steinmetz, Classical Model and Improve Core Loss Model Comparison

An improved formula with a physical basis for the variation of loss coefficients with flux density and/or frequency developed by Lotten in using the test bench results is presented and tested here. Furthermore, an alternative averaging method of excess loss coefficient is presented as a modification in order to reduce the computation time. The new formula is an extension of Bertotti's formula in (32) addressing the shortcomings observed in [Figures .5.5(d)]and testing under non-sinusoidal flux density waveforms. The improved formula has good accuracy at high flux densities and frequencies, and takes a form of equation (32) The eddy current and excess loss coefficients k_e and k_{ex} are allowed to vary with frequency and with flux density. Variation of k_e with frequency accounts for skin effects at higher

frequencies, this is especially important for thick materials. The excess loss coefficient varies with both flux density and frequency since flux density in the lamination is not uniform - contrary to what is commonly assumed. Moreover, at higher frequencies, the skin effect prevents flux from penetrating through the lamination. Hence, qualitatively, the dependence of k_{ex} on both frequency and flux density represents physical reality. It has been shown by Steinmetz in that hysteresis losses per cycle does not vary significantly with frequency, hence extrapolating the P/f (total loss divided by frequency vs. frequency) curve in **[Figure 5.5(d)]** to zero frequency to determine hysteresis loss is justified. In this way, the material and operational dependence of n , the Steinmetz's constant, and k_h are implicitly included in the formula.

CHAPTER 7: CONCLUSIONS

7. CONCLUSIONS:

1. The Steinmetz and classical formulae predict the same core losses at various frequencies and materials provided the loss coefficients are recalculated at frequency of concern.
2. The skin effect must be accounted for when using classical formula at high frequencies. Limited loss data affect loss prediction at higher frequencies, resulting in a significant deviation from measurements, especially for the classical formula.
3. The Steinmetz constant, $n = 1.6$, is not generically applicable to all materials. The modified Steinmetz model does not necessary predict better results than the original Steinmetz's formula, especially at high flux densities.
4. Bertotti's formula shows improvement when compared to the classical model with physical basis, especially when estimation is done with limited loss data. However, Bertotti's formula still under estimates losses at high flux densities. Also, the formula is invalid at high frequencies.

Chapter 8: FUTURE SCOPE

8. Future scope

- 1) Without dissipation of energy, we can make a core which is more effective.
- 2) Although the magnetic flux density of ferromagnetic material is higher than ferrites, they exhibit too much core loss. If we can control the losses in those alloys, we can fabricate magnetic core devices of smaller size than ferrite core
- 3) Since ferro-magnetic materials are made up with iron (Fe) and very less amount of other components, so we can reduce the cost of magnetic core.

CHAPTER 9: REFERENCE

9. Reference

- Adler, E., 1989. Matching P/M and the physics of magnetic materials. *Int. J. Powder Met*, 25, pp.319-335.
- Arnold, H.D. and Elmen, G.W., 1923. Permalloy, a new magnetic material of very high permeability. *Bell System Technical Journal*, 2(3), pp.101-111.
- Balci, S., Sefa, I. and Bayram, M.B., 2014, September. Core material investigation of medium-frequency power transformers. In *2014 16th International Power Electronics and Motion Control Conference and Exposition* (pp. 861-866). IEEE.
- Bertotti, G., 1984. A general statistical approach to the problem of eddy current losses. *Journal of magnetism and Magnetic Materials*, 41(1-3), pp.253-260.
- Bertotti, G., 1998, *Hysteresis in magnetism: for physicists, materials scientists, and engineers*. Gulf Professional Publishing.
- Boglietti, A., Cavagnino, A., Lazzari, M. and Pastorelli, M., 2003. Predicting iron losses in soft magnetic materials with arbitrary voltage supply: An engineering approach. *IEEE Transactions on magnetics*, 39(2), pp.981-989.
- Brighenti, L.L., Martins, D.C. and Dos Santos, W.M., 2019, June. Study of magnetic core geometries for coupling systems through a magnetic bus. In *2019 IEEE 10th International Symposium on Power Electronics for Distributed Generation Systems (PEDG)* (pp. 29-36). IEEE.
- Carr Jr, W.J. and Smoluchowski, R., 1951. The magnetostriction of single crystals of iron-silicon alloys. *Physical Review*, 83(6), p.1236.
- Cullity, B.D. and Graham, C.D., 2011. *Introduction to magnetic materials*. John Wiley & Sons.
- de Vries, M.J., 80. Years of Research at Philips. The History of the Philips Natuurkundig Laboratorium, 1914-1994. *Eindhoven: Stichting Historie der Techniek*.

Della Torre, E., Pinzaglia, E. and Cardelli, E., 2006. Vector modeling—Part II: Ellipsoidal vector hysteresis model. Numerical application to a 2D case. *Physica B: Condensed Matter*, 372(1-2), pp.115-119.

Ducharne, B., Tsafack, P., Deffo, Y.T., Zhang, B. and Sebald, G., 2021. Anomalous fractional magnetic field diffusion through cross-section of a massive toroidal ferromagnetic core. *Communications in Nonlinear Science and Numerical Simulation*, 92, p.105450.

Ducharne, B., Tsafack, P., Deffo, Y.T., Zhang, B. and Sebald, G., 2021. Anomalous fractional magnetic field diffusion through cross-section of a massive toroidal ferromagnetic core. *Communications in Nonlinear Science and Numerical Simulation*, 92, p.105450.

Duwez, P. and Lin, S.C.H., 1967. Amorphous ferromagnetic phase in iron-carbon-phosphorus alloys. *Journal of Applied Physics*, 38(10), pp.4096-4097.

García-Cerda, L.A., Rodríguez-Fernández, O.S. and Reséndiz-Hernández, P.J., 2004. Study of SrFe₁₂O₁₉ synthesized by the sol–gel method. *Journal of alloys and compounds*, 369(1-2), pp.182-184.

Gavrila, H. and Ionita, V., 2002. Crystalline and amorphous soft magnetic materials and their applications- status of art and challenges. *Journal of Optoelectronics and Advanced Materials (Romania)*, 4(2), pp.173-192.

Goldman, A., 2006. Ferrite processing. *Modern Ferrite Technology*, pp.151-216.

Graham Jr, C.D., 1982. Physical origin of losses in conducting ferromagnetic materials. *Journal of Applied Physics*, 53(11), pp.8276-8280.

Graham Jr, C.D., 1982. Physical origin of losses in conducting ferromagnetic materials. *Journal of Applied Physics*, 53(11), pp.8276-8280.

Graham, C.D., 2009. *Physics of ferromagnetism*. OUP.

Hall, R.C., 1959. Single crystal anisotropy and magnetostriction constants of several ferromagnetic materials including alloys of NiFe, SiFe, AlFe, CoNi, and CoFe. *Journal of Applied Physics*, 30(6), pp.816-819.

Hamann,D.I.C., 2010. Magnetische Hybridschichten-Magnetische Eigenschaften lokal austauschgekoppelter NiFe/IrMn-Schichten.

Hasani, S., Shafyei, A., Shamanian, M., Behjati, P., Mostaan, H., Juuti, T. and Szpunar, J.A., 2015. Correlation between magnetic properties and allotropic phase transition of Fe–Co–V alloy. *Acta Metallurgica Sinica (English Letters)*, 28, pp.1055-1058.

Huo, X.T.B., 2009. New model of eddy current loss calculation and applications for partial core transformers.

Iniewski, K., 2012. *Advanced circuits for emerging technologies*. John Wiley & Sons.

Ishikura, Y., Imaoka, J., Noah, M. and Yamamoto, M., 2018, May. Core loss evaluation in powder cores: A comparative comparison between electrical and calorimetric methods. In *2018 International Power Electronics Conference (IPEC-Niigata 2018-ECCE Asia)* (pp. 1087-1094). IEEE.

Jack, A.G., Mecrow, B.C., Dickinson, P.G., Stephenson, D., Burdess, J.S., Fawcett, N. and Evans, J.T., 2000. Permanent-magnet machines with powdered iron cores and prepressed windings. *IEEE Transactions on industry applications*, 36(4), pp.1077-1084.

Jafari, M., Malekjamshidi, Z. and Zhu, J., 2017, August. Accurate copper loss analysis of a multi-winding high-frequency transformer for a magnetically-coupled residential micro-grid. In *2017 20th International Conference on Electrical Machines and Systems (ICEMS)* (pp. 1-6). IEEE.

Jančárik, V., Grusková, A., Sláma, J. and Dosoudil, R., 2006. Study of Sr and Ba hexaferrite prepared by low temperature auto-combustion method. *J. Electr. Eng.*, 57(8/S), pp.163-166.

Jiandong, D., Yang, L. and Hao, L., 2018, November. Research on ferromagnetic components Ja model-a review. In *2018 International Conference on Power System Technology (POWERCON)* (pp. 3288-3294). IEEE.

Jiles, D., 2015. *Introduction to magnetism and magnetic materials*. CRC press.

Kasai, S., Namikawa, M. and Hiratani, T., 2016. Recent progress of high silicon electrical steel in JFE steel. *JFE Tech. Rep*, 21(03), pp.14-19.

Landau, L.A.L.E. and Lifshitz, E., 1992. On the theory of the dispersion of magnetic permeability in ferromagnetic bodies. In *Perspectives in Theoretical Physics* (pp. 51-65). Pergamon.

Manyage, M.J. and Pillay, P., 2007, September. Low voltage high current PM traction motor design using recent core loss results. In *2007 IEEE Industry Applications Annual Meeting* (pp. 1560-1566). IEEE.

Martins, S., Seidel, Á.R., Perdigão, M.S. and Roggia, L., 2022. Core volume reduction based on non-linear inductors for a PV DC–DC converter. *Electric Power Systems Research*, 213, p.108716.

McHenry, M.E. and Laughlin, D.E., 2000. Nano-scale materials development for future magnetic applications. *Acta materialia*, 48(1), pp.223-238.

Mthombeni, T.L. and Pillay, P., 2006, November. Physical basis for the variation of lamination core loss coefficients as a function of frequency and flux density. In *IECON 2006-32nd Annual Conference on IEEE Industrial Electronics* (pp. 1381-1387). IEEE.

Mthombeni, T.L., 2006. *Improved lamination core loss measurements and calculations* (Doctoral dissertation, Clarkson University).

Ouyang, G., Chen, X., Liang, Y., Macziewski, C. and Cui, J., 2019. Review of Fe-6.5 wt% Si high silicon steel—A promising soft magnetic material for sub-kHz application. *Journal of Magnetism and Magnetic Materials*, 481, pp.234-250.

Paimozd, E., Ghasemi, A., Jafari, A. and Sheikh, H., 2008. Influence of acid catalysts on the structural and magnetic properties of nanocrystalline barium ferrite prepared by sol–gel method. *Journal of magnetism and magnetic materials*, 320(23), pp. L137-L140.

Parthasaradhy, P. and Ranganayakulu, S.V., 2014. Hysteresis and eddy current losses of magnetic material by Epstein frame method-novel approach. *The International Journal of Engineering and Science*, pp.85-93.

- Ram, B.S. and Kulkarni, S.V., 2019. An isoparametric approach to model ferromagnetic hysteresis including anisotropy and symmetric minor loops. *Journal of Magnetism and Magnetic Materials*, 474, pp.574-584.
- Rodríguez-Sotelo, D., Rodríguez-Licea, M.A., Araujo-Vargas, I., Prado-Olivarez, J., Barranco-Gutiérrez, A.I. and Pérez-Pinal, F.J., 2022. Power losses models for magnetic cores: A review. *Micromachines*, 13(3), p.418.
- Rodríguez-Sotelo, D., Rodríguez-Licea, M.A., Araujo-Vargas, I., Prado-Olivarez, J., Barranco-Gutiérrez, A.I. and Pérez-Pinal, F.J., 2022. Power Losses Models for Magnetic Cores: A Review. *Micromachines* 2022, 13, 418.
- Rodríguez-Sotelo, D., Rodríguez-Licea, M.A., Soriano-Sanchez, A.G., Espinosa-Calderon, A. and Pérez-Pinal, F.J., 2020. Advanced ferromagnetic materials in power electronic converters: A state of the art. *IEEE Access*, 8, pp.56238-56252.
- Saeed, S., Georgious, R. and Garcia, J., 2020. Modeling of magnetic elements including losses—Application to variable inductor. *Energies*, 13(8), p.1865.
- Sato, M. and Ishii, Y., 1989. Simple and approximate expressions of demagnetizing factors of uniformly magnetized rectangular rod and cylinder. *Journal of Applied Physics*, 66(2), pp.983-985.
- Sauthoff, G., 2002. References for 14: 14 Intermetallic materials. *Powder Metallurgy Data. Refractory, Hard and Intermetallic Materials*, pp.258-265.
- Steinmetz, C.P., 1892. On the law of hysteresis. *Transactions of the American Institute of Electrical Engineers*, 9(1), pp.1-64.
- Sun, H., Li, Y., Lin, Z., Zhang, C. and Yue, S., 2020. Core loss separation model under square voltage considering DC bias excitation. *AIP Advances*, 10(1).
- Tan, F.D., Vollin, J.L. and Cuk, S.M., 1995. A practical approach for magnetic core-loss characterization. *IEEE Transactions on Power Electronics*, 10(2), pp.124-130.

Tan, F.D., Vollin, J.L. and Cuk, S.M., 1995. A practical approach for magnetic core-loss characterization. *IEEE Transactions on Power Electronics*, 10(2), pp.124-130.

Tatsumoto, E. and Okamoto, T., 1959. Temperature dependence of the magnetostriction constants in iron and silicon iron. *Journal of the Physical Society of Japan*, 14(11), pp.1588-1594.

Weiss, P., 1907. Hypothesis of the molecular field and ferromagnetic properties. *J. phys*, 4(6), pp.661-690.

Williams, H.J., Shockley, W. and Kittel, C., 1950. Studies of the propagation velocity of a ferromagnetic domain boundary. *Physical Review*, 80(6), p.1090.

Yoshizawa, Y.A., Oguma, S. and Yamauchi, K., 1988. New Fe-based soft magnetic alloys composed of ultrafine grain structure. *Journal of applied Physics*, 64(10), pp.6044-6046.

Yue, S., Li, Y., Yang, Q., Yu, X. and Zhang, C., 2018. Comparative analysis of core loss calculation methods for magnetic materials under non sinusoidal excitations. *IEEE transactions on magnetics*, 54(11), pp.1-5.

Zhao, X., Liu, X., Zhao, Z., Zou, X., Xiao, Y. and Li, G., 2019. Measurement and modeling of hysteresis characteristics in ferromagnetic materials under DC magnetizations. *AIP Advances*, 9(2).

Zhukov, A., Vázquez, M., Velázquez, J., Garcia, C., Valenzuela, R. and Ponomarev, B., 1997. Frequency dependence of coercivity in rapidly quenched amorphous materials. *Materials Science and Engineering: A*, 226, pp.753-756.